

# Zwitterionic polymers-armed amyloid-like protein surface combats thrombosis and biofouling

Xiaohui Mou<sup>a,b</sup>, Wan Miao<sup>a</sup>, Wentai Zhang<sup>b</sup>, Wenxuan Wang<sup>a</sup>, Qing Ma<sup>a,b</sup>, Zeyu Du<sup>a,b</sup>, Xin Li<sup>c</sup>, Nan Huang<sup>a,\*\*</sup>, Zhilu Yang<sup>b,c,\*</sup>

<sup>a</sup> School of Materials Science and Engineering, Key Lab of Advanced Technology of Materials of Education Ministry, Southwest Jiaotong University, Chengdu, 610031, China

<sup>b</sup> Dongguan Key Laboratory of Smart Biomaterials and Regenerative Medicine, The Tenth Affiliated Hospital of Southern Medical University, Dongguan, Guangdong, 523000, China

<sup>c</sup> Department of Cardiology, Third People's Hospital of Chengdu Affiliated to Southwest Jiaotong University, Chengdu, Sichuan 610072, China

## ARTICLE INFO

### Keywords:

Amyloid-like protein  
Antifouling  
Antithrombosis  
Super-Hydrophilicity  
Zwitterionic polymers

## ABSTRACT

Proteins, cells and bacteria adhering to the surface of medical devices can lead to thrombosis and infection, resulting in significant clinical mortality. Here, we report a zwitterionic polymers-armed amyloid-like protein surface engineering strategy we called as “armored-tank” strategy for dual functionalization of medical devices. The “armored-tank” strategy is realized by decoration of partially conformational transformed LZM (PCTL) assembly through oxidant-mediated process, followed by armoring with super-hydrophilic poly-2-methacryloyloxyethyl phosphorylcholine (pMPC). The outer armor of the “armored-tank” shows potent and durable zone defense against fibrinogen, platelet and bacteria adhesion, leading to long-term antithrombogenic properties over 14 days *in vivo* without anticoagulation. Additionally, the “fired” PCTL from “armored-tank” actively and effectively kills both Gram-positive and Gram-negative bacterial over 30 days as a supplement to the lacking bactericidal functions of passive outer armor. Overall, this “armored-tank” surface engineering strategy serves as a promising solution for preventing biofouling and thrombotic occlusion of medical devices.

## 1. Introduction

Indwelling medical devices, such as catheters and needles, as well as extracorporeal circuits, are extensively used in various medical treatments, including hemodialysis [1], drug delivery [2], extracorporeal circulation [3] and other clinical treatments [4–6]. However, these devices are still challenged by thrombosis and infections, which commonly result in serious complications [7–10]. To address these issues, anticoagulants and antibiotics have been commonly used in clinical practice over the past few decades. Nevertheless, long-term administration of these agents has been associated with potential adverse effects, including hemorrhage [11], antibiotic resistance [12], thrombophlebitis [13], and hepatic overload [14]. In recent years, surface engineering approaches are attracting increasing attention in the field of

blood-contacting medical devices. Such approaches involve modifying and enhancing the device surfaces to achieve specific functionalities and interactions *in situ*, such as anticoagulant and antibacterial surfaces [15–19], which provides distinct advantages in addressing the clinical complications associated with implanted devices.

Current surface engineering strategies for anticoagulant and antimicrobial purposes can be broadly categorized into two approaches: active attack and zone defense [20]. The active attack strategy involves the integration of bioactive molecules (e.g., antibiotics [21], peptide [22], chitosan [23] and anticoagulants [24]) onto the surfaces of devices. These molecules combat bacteria or inhibit platelet activation by releasing them *in situ*. However, such strategies have limitations in regulating the adsorption of blood proteins and bacteria on the device surface, which can trigger undesired biological responses, such as

Peer review under responsibility of KeAi Communications Co., Ltd.

\* Corresponding author. Dongguan Key Laboratory of Smart Biomaterials and Regenerative Medicine, The Tenth Affiliated Hospital of Southern Medical University, Dongguan, Guangdong, 523000, China.

\*\* Corresponding author. School of Materials Science and Engineering, Key Lab of Advanced Technology of Materials of Education Ministry, Southwest Jiaotong University, Chengdu, 610031, China.

E-mail addresses: [huangnan1956@163.com](mailto:huangnan1956@163.com) (N. Huang), [zhiluyang1029@smu.edu.cn](mailto:zhiluyang1029@smu.edu.cn) (Z. Yang).

<https://doi.org/10.1016/j.bioactmat.2023.09.003>

Received 4 August 2023; Received in revised form 6 September 2023; Accepted 6 September 2023

2452-199X/© 2023 The Authors. Publishing services by Elsevier B.V. on behalf of KeAi Communications Co. Ltd. This is an open access article under the CC BY-NC-ND license (<http://creativecommons.org/licenses/by-nc-nd/4.0/>).

platelet adhesion and bacterial colonization. This affects the releasing of bioactive molecules, further resulting in infections and biofilm-related complications. On the other hand, the zone defense strategy [25] prevents the adsorption of blood proteins by covalent immobilization of protein-resistant polymers, including poly-(ethylene glycol) (PEG) [26], zwitterionic polymers [27], hyaluronic acid (HA) [28] and heparin [29], on the surfaces of devices. These protein-resistant surfaces efficiently inhibit platelet adhesion and bacterial colonization. Unfortunately, passive anti-fouling surfaces tend to gradually lose their effectiveness over time, especially in complex pathological environments [30]. It is important to note that even a minimal amount of bacteria adsorption on the surface is sufficient to initiate the proliferation of undesirable fouling [31,32], finally causing the formation of biofilm on devices. Additionally, the presence of biofilms further induces thrombus formation, leading to device failure. Therefore, relying solely on single zone defense or active attack strategies may not be sufficient to construct a durable and effective anti-fouling surface.

Herein, we proposed a zwitterionic polymers-armed amyloid-like protein surface engineering strategy, called “armored-tank” strategy,

which combined the zone defense and active attack strategies to provide long-term antibacterial and anticoagulant capabilities to extracorporeal circuits and indwelling medical devices (Fig. 1). The concept of the “armored tank” served as an analogy to illustrate the effectiveness of this approach. Similar to an “armored tank” equipped with robust “armor” and powerful “firepower systems”, our approach simultaneously attacked bacteria while being shielded by a strong anti-adhesive armor. To implement this strategy, we employed lysozyme (LZM), a protein known for its antimicrobial properties [33], to create a partially conformational transformed LZM (PCTL) assembly through oxidant-mediated. The PCTL assembly exhibited excellent biocompatibility, strong adhesion to various materials, and potent antimicrobial activity, serving as the “firepower system” of the “armored tank” for active attack bacterial. Given the occurrence of biofilm formation resulting from the unavoidable adsorption of bacteria onto the surface of PCTL assembly, an additional protection armor for PCTL assembly was further implemented to ensure the bactericidal efficacy of PCTL. To armor the amyloid-like PCTL assembly, N-Hydroxysuccinimide acrylate (NAS) was grafted onto PCTL assembly through carbodiimide chemistry,

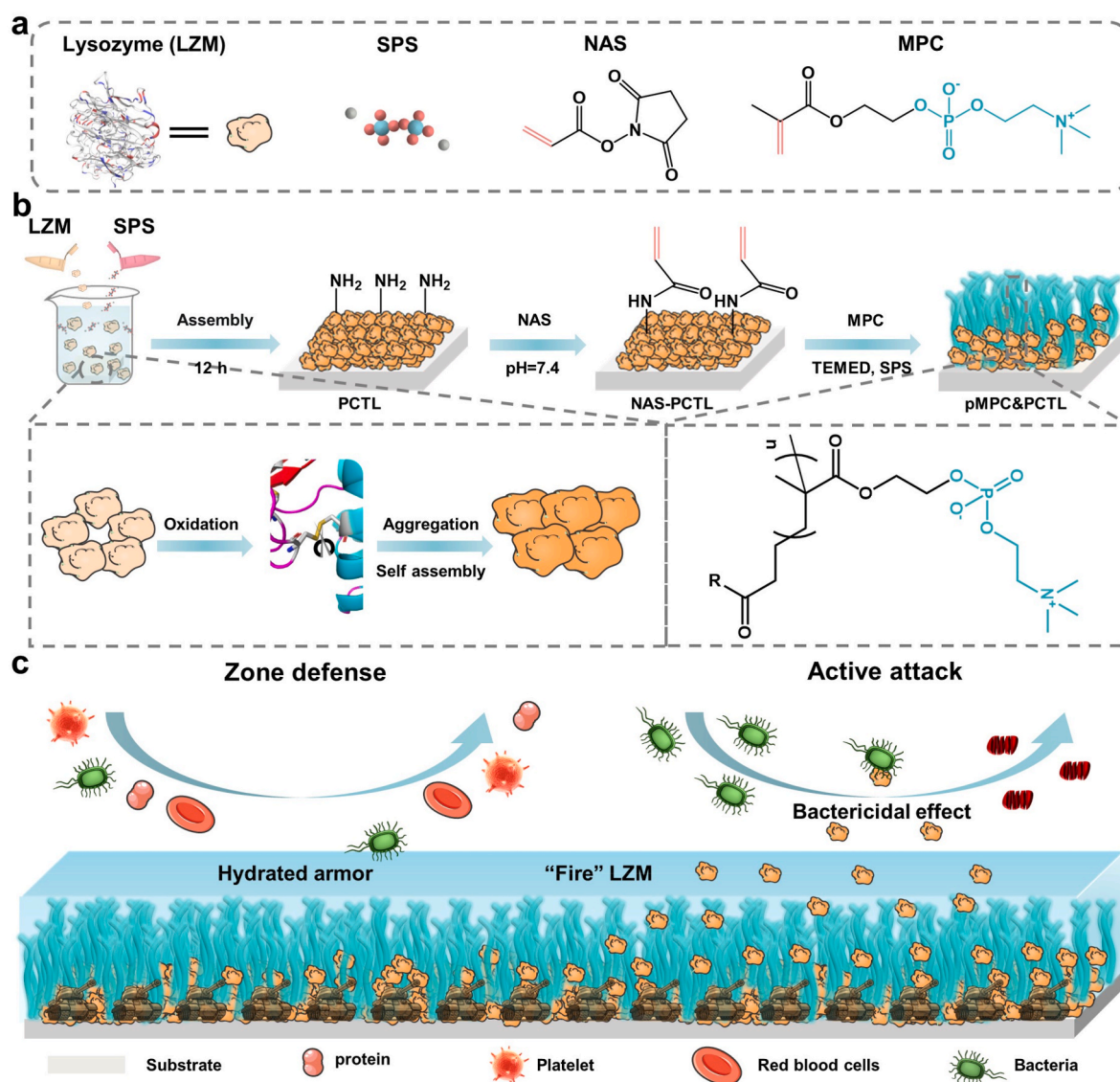


**Fig. 1.** Schematic illustration of pMPC&LZM “armored-tank” with anticoagulation and antibacterial properties. (a) Chemical structure of the lysozyme (LZM), sodium persulfate (SPS), N-Hydroxysuccinimide acrylate (NAS) and 2-Methacryloyloxyethyl phosphorylcholine (MPC). (b) Armorization on representative medical devices through carbodiimide chemistry and free radical polymerization reaction. (c) Realization of anticoagulation and synergistic antibacterial properties of pMPC&LZM “armored-tank”.

introducing an active carbon-carbon double bond for subsequent *in-situ* free radical polymerization. Finally, 2-methacryloyloxyethyl phosphorylcholine (MPC), a zwitterionic molecule as a major constituent in the cellular membranes [34], was polymerized to form a super-hydrophilic poly-MPC (pMPC) molecular brush through *in-situ* free radical polymerization. This pMPC zwitterionic molecular brush acted as a protective “armor” of the “armored-tank”, effectively inhibiting protein and bacterial adhesion. The synergy between the “fire-power system” (specifically, LZM releasing for active attack) and “armor” (specifically, super-hydrophilic pMPC molecular brush for zone defense) in this design endowed the engineered surface with highly persistent anticoagulant and antibacterial capabilities. We envisioned that this integrated “armored-tank” strategy, combining active attack and zone defense, holds great promise as a solution for effectively addressing thrombosis and biofouling on surfaces in various biomedical applications.

## 2. Experimental methods

### 2.1. Materials

Egg white lysozyme (LZM), Sodium persulfate (SPS), phosphate buffered saline (PBS), Bacterial Activity Detection Kit (LIVE/DEAD BacLight, Thermo Fisher Scientific), 1-Anilinonaphthalene 8-sulfonate (ANS), Thioflavin-T (ThT), Glutaraldehyde, Rhodamine 6G, N-Hydroxysuccinimide acrylate (NAS), Dimethyl sulfoxide (DMSO), Sodium hydroxide (NaOH), 2-Methacryloyloxyethyl phosphorylcholine (MPC), N, N,N',N'-Tetramethylethylenediamine (TEMED), Bacterial culture medium, were purchased from Sigma-Aldrich. All these materials were used as received. All solutions were freshly prepared for immediate use in each experiment.

### 2.2. Preparation of PCTL assembly

To enhance the adhesion between the coating and the substrate material, the Polyurethane (PU) wafer (1 cm<sup>2</sup> for antiplatelet test and 2 cm<sup>2</sup> for antibacterial assessment) and catheters (inner diameter  $\Phi = 3.0$  mm) were sputtered with plasma for 10 min. Then, the prepared PU wafer and catheters were immersed in an aqueous solution of sodium persulfate (2 mg/mL) mixed in equal volume with LZM aqueous solution (1 mg/mL, buffered by 1 mM of NaOH, pH 5). After 12 h of standing reaction at 37 °C, the PU substrates were ultrasonically cleaned with distilled water and dried by nitrogen gas (N<sub>2</sub>) for future use, marked as PCTL. To achieve a more uniform coating, repeat the film deposition process three times. For ellipsometric analysis, sequential buildup of PCTL coatings was performed on silicon wafers prepared immediately prior to use.

### 2.3. CD spectroscopy for natural LZM and PCTL assembly

After incubating for different durations at room temperature, the natural LZM and PCTL samples prepared with different APS concentration were introduced into a quartz plate (path length: 0.1 mm, volume: 3 mL) and analyzed using a spectropolarimeter (Jasco, J-1500 CD Spectrometer). The CD spectra (range: 190 - 260 nm, interval: 1 nm) were calculated from the averaged value of three scans (10 nm min<sup>-1</sup>), which were smoothed by the software provided by the manufacturer of the equipment.

### 2.4. ANS fluorescence staining of natural LZM and PCTL assembly

To assess the extent of hydrophobic residue exposure in the assembly of PCTL, ANS was employed as a fluorescent probe. A protein solution (2 mL, 1 mg/mL) was mixed with ANS (300  $\mu$ L, 100  $\mu$ M) at room temperature for a duration of 2 h (while being shielded from light). And then, APS (0 and 500  $\mu$ L, 100  $\mu$ M) were introduced into the mixed

solution. Subsequently, ANS fluorescence was measured using a FLS-920 fluorescence spectrophotometer (Edinburgh Instruments) by recording emission spectra at 480 nm with excitation at 355 nm.

### 2.5. Preparation of NAS-PCTL and PCTL&pMPC surface

Firstly, the PCTL-modified PU substrates or catheters were firstly immersed into 3 mg/mL solution of NAS dissolved in a solvent consisting of 95% phosphate-buffered saline (PBS) and 5% dimethyl sulfoxide (DMSO) for 12 h at room temperature, and then rinsed by distilled water and dried with a stream of N<sub>2</sub>. The resulting NAS-modified surface was named as “NAS-PCTL”. Subsequently, the NAS-PCTL-modified PU was incubated with 50 mg/mL MPC solution dissolved in a solvent containing of SPS (20 mg/mL) with added TEMED (8  $\mu$ L/mL). This reaction process lasted for 24 h in an N<sub>2</sub> environment, leading to the preparation of the pMPC armor, which was named as “pMPC&PCTL”. After grafting, the substrates or tubes were rinsed thoroughly with distilled water and dried with N<sub>2</sub> gas for further use.

### 2.6. Characterization

Scanning electron microscope (SEM) (JSF700) were used to investigate surface morphology of coating. To determine the thickness of coatings, a spectroscopic ellipsometer (W-VASE, J.A. Woollam, USA) was carried out. Considering the rough surface of the PU substrate, it was still challenging to accurately measure the thickness of the pMPC&PCTL surface. As a result, silicon substrates were employed instead of PU substrates to deposit. The water contact angle (WCA) of samples was measured using a DSA100 drop shape analysis system (KRuSS GmbH Company, Hamburg, Germany). Fourier transform infrared (FTIR) spectra were collected using a Nicolet model 5700 instrument. X-ray photoelectron spectroscopy (XPS) (K-alpha, Thermo-Fisher, USA) was used to understand the chemical information of the surface. Ellipsometer (Sopra GES-5E, Courbevoie, France) was employed to measure the thickness of surfaces. Additionally, The LZM concentration in the eluent obtained from the pMPC&PCTL surfaces after PBS treatment with different days (1,3 and 7 days), was determined by ultraviolet absorption (UV-vis spectroscopy, UV-2550, Shimadzu). The concentration of LZM was then calculated by referencing a standard curve created from measurements of LZM at various concentrations.

### 2.7. Quantification of amino groups

The acid Orange colorimetric method was employed to quantify the concentration of amino groups, including primary, secondary, and tertiary amines, on the surface. Briefly, the samples were immersed in an acid Orange II (AO II) solution (pH 3) for 12 h at 37 °C. Subsequently, the samples were rinsed with a HCl solution (pH 3) to remove any unreacted AO II, followed by drying with nitrogen gas. Afterward, a NaOH solution (pH 12, 200  $\mu$ L) was applied to the sample surface for 15 min to release AO II, which was bound through electrostatically. The concentration of AO II in the NaOH solution was determined at 485 nm using an enzyme marker ( $\mu$ Quant, Bio-tek Instruments Inc.). The density of the amine groups was then calculated by using a standard curve based on measurements of AO II at different concentrations.

### 2.8. Antibacterial activity

The antibacterial activity of the surfaces was tested using Gram-positive bacteria (*S. epidermidis*) and Gram-negative bacteria (*E. coli*), as previously described in our work [35]. The inhibition of *S. epidermidis* and *E. coli* was used as indicators the antibacterial efficacy of the pMPC&PCTL surfaces. Initially, *E. coli* and *S. epidermidis* bacteria were cultured on agar solid medium at 37 °C for 24 h. The bacteria were then sub-cultured twice to ensure monoclonality. Subsequently, fresh bacterial colonies consisting of 1 - 2 rings were selected and dispersed in a

solution comprising 0.2% liquid medium and 99.8% saline. The concentration of the bacteria was adjusted to a range of  $5.0 \times 10^5$  to  $10^6$  CFU mL<sup>-1</sup> through a series of tenfold dilutions. A volume of 200  $\mu$ L of the aforementioned bacterial solution was applied onto the sample surface and covered with a soft polyethylene (PE) membrane to ensure an even liquid film spread over the substrate. The samples were incubated at 37 °C. The bacteria on the surfaces were rinsed and dissolved in a saline solution measuring 2 mL after 24 h culture period. Subsequently, 20  $\mu$ L of this bacterial solution was evenly distributed onto the solid medium and cultured for an additional 24 h at 37 °C. Ultimately, the colonies on the solid medium were counted. To observe the adherence of bacteria on the sample surface, a volume of 500  $\mu$ L of the aforementioned bacterial solution was applied onto the sample surface. After 24 h culture period at 37 °C, the bacteria present on the surfaces were slightly rinsed with saline solution and subsequently fixed overnight using a 2.5% glutaraldehyde solution. After further dehydration and dealcoholisation, the bacteria adhered to the surfaces of the samples were observed using a scanning electron microscope (SEM). Additionally, antibacterial assays were performed using the eluent obtained from the pMPC&PCTL surface. Briefly, the eluent obtained from the pMPC&PCTL surface exposed to PBS for different durations (1, 3 and 7 days), was collected to assess its effect on bacterial growth and viability. In this process, the solution was replaced every 72 h.

## 2.9. In vitro hemocompatibility evaluation

Fresh blood samples were obtained from healthy adult New Zealand white rabbits. Platelet-rich plasma (PRP) and platelet-poor plasma (PPP) were prepared as previously described procedures [36]. To assess the anticoagulation performance of the pMPC&PCTL surfaces, fibrinogen/platelet adhesion and activation experiments were conducted. Briefly, fibrinogen (Fg) adsorption test was conducted by applying PPP (50  $\mu$ L) onto the samples at 37 °C for 2 h. The samples were then rinsed with PBS. Subsequently, HRP-labeled sheep PAb anti-human fibrinogen (Sigma-Aldrich) was subsequently added (20  $\mu$ L) and incubated for 60 min. Following this, a chromogenic substrate solution, specifically 3,3', 5,5'-tetramethylbenzidine (TMB) (100  $\mu$ L), was added. Ten minutes later, the reaction was terminated by introducing an acid solution, and the absorbance was measured at 405 nm. Regarding the activation of Fg, the samples were first incubated with PPP for 120 min. Subsequently, the samples were washed using PBS and then treated with a mouse anti-human  $\gamma$ -fibrinogen monoclonal antibody (20  $\mu$ L) at 37 °C for 1 h. The sample was washed and then exposed to a sheep anti-mouse polyclonal antibody labeled with horseradish peroxidase (HRP) (20  $\mu$ L). Afterward, a solution of tetramethylbenzidine (TMB) (100  $\mu$ L) was introduced and incubated for a period of 10 min. The measurement of absorbance at a wavelength of 405 nm was conducted subsequent to the addition of an acid solution supplement.

Subsequently, the substrates were incubated with 0.5 mL of platelet-rich plasma (PRP) at 37 °C for 30 min. Subsequently, the substrates were rinsed thrice with a saline solution and subsequently fixed overnight using a 2.5% glutaraldehyde solution. After further dehydration and dealcoholisation, the platelets adhered to the surfaces of the samples were observed using a SEM (JSF 700).

## 2.10. Ex vivo thrombogenicity

All animal experiments were approved by the Dongguan People's Hospital Laboratory Animal Welfare and Ethics Committee (Approval NO. IACUC-AWEC-202210001). To evaluate the antithrombogenic properties of the pMPC&PCTL surfaces in circulation, an *ex vivo* blood circuits experiment was further carried out [37]. In this study, a total of four adult New Zealand white rabbits weighing between 2.2 and 2.5 kg were anesthetized using pentobarbital sodium at a concentration of 30 mg/mL, with a dosage of 1 mL per kg. The left carotid artery and right external jugular vein were surgically exposed and cannulated.

Subsequently, a PU catheter was connected to the cannulas to establish a closed loop system. After undergoing *ex vivo* circulation for a duration of 2 h, the unmodified, PCTL-modified, NAS-PCTL-modified, and pMPC&PCTL-modified PU tubings were removed and rinsed with saline solution three times. The occlusive rates of the tubings were determined by examining the cross-sections. Additionally, the blood flow rate at *t* at the end of the circulation period was also measured.

## 2.11. Blood analysis by ex vivo blood circulation

For the blood analysis after *ex vivo* blood circulation, a total of eight adult New Zealand white rabbits were utilized in this study. Each rabbit received only one circuit, either unmodified PU tubing or pMPC&LZM-modified tubing. Blood samples were collected at different time intervals (0, 5, 30, and 60 min) from the running circulation for the analysis. It is worth noting that, to mitigate the potential influence of the vascular puncture process on blood analyses, we collected initial blood samples prior to vascular puncture, thus establishing a baseline control group (0 min time point). The blood analysis included activated partial thromboplastin time (APTT), prothrombin fragment 1 + 2 (F1+2), complement component 3a (C3a), C-reactive protein (CRP), white blood cell count (WBC), platelet count (PLT), interleukin-10 (IL-10), tumor necrosis factor-alpha (TNF- $\alpha$ ), alanine aminotransferase (ALT), and creatinine (CRE). To obtain plasma and serum, a portion of the freshly collected whole blood was centrifuged at 2500 rcf for 15 min with and without anticoagulants, respectively. In order to evaluate the potential impact of the coated catheter on blood composition and liver and kidney functions, a single prolonged catheter was selected to simulate clinical application. Considering the significantly larger total blood volume in adult humans compared to mature white rabbits (~200 mL for mature white rabbits and ~4000 mL for adult humans), a 1.6-m-long PU tube with an inner diameter of 3 mm was chosen for modifying the lumen surface. This selection allowed for an enlarged contact area, facilitating the examination of the differential effects between the modified and unmodified (control) catheter. The APTT was measured using the manual tilt-tube method (13). ELISA kits (Rabbit CRP/TNF- $\alpha$ /C3a/IL-10/F1+2 ELISA KIT, ZC-52314/ZC-52984/ZC-52409/ZC-52381/ZC-52601, Shanghai ZCIBIO Technology Co.,Ltd.) were employed to measure CRP, TNF- $\alpha$ , C3a, IL-10, and F1+2 levels according to the manufacturer of specifications. WBC and PLT counts were determined using an animal automatic blood cell analyzer (Shenzhen Mindray, BC-2800Vet), while ALT and creatinine (Scr) levels were measured using an animal biochemical analyzer (Shenzhen Mindray, BS-240VET).

## 2.12. Evaluate the long-term stability of the pMPC&PCTL surfaces

To evaluate the long-term antibacterial and antithrombogenic properties of the pMPC&PCTL surfaces, the samples were pre-immersed in a PBS solution. This solution was replaced every three days. Samples were established for different time points, including 0, 1, 3, 5, 7, 15, 21 and 30 days, to conduct characterization (e.g., Chemical composition, Thickness, Water contact Angle), antibacterial experiments and *ex vivo* circulation experiments.

## 2.13. Statistical analysis

The results are presented as the mean  $\pm$  standard deviation of the mean for each sample. All experiments were independently repeated at least three times, unless otherwise specified. Statistical analysis was performed using one-way analysis of variance (ANOVA) and Student's *t*-test in GraphPad Prism 8.0 software (GraphPad Prism Software, San Diego, CA, USA) to compare data between different groups.

### 3. Results and discussion

#### 3.1. Fabrication and characterization of PCTL

Amyloid-like proteins have garnered attention as promising candidates for bio-inspired coatings due to their distinct  $\beta$ -sheet structures [38]. These structures offer excellent resistance to high temperatures, organic solvents, and harsh pH conditions, making them highly desirable for various applications [39–42]. Previous studies have suggested a potential link between reactive oxygen species (ROS) and the development and accumulation of amyloid-like protein. ROS initiates protein oxidation and trigger changes in protein structure, ultimately promoting the aggregation of amyloid-like proteins [43]. Inspired by this, herein, we developed a partially conformation transitioned LZM (PCTL) assembly by employing ammonium persulfate (APS, oxidizing agent) to break down the disulfide bond of LZM. This process further induced heterogeneous nucleation and assembly of active LZM onto the surface of substrates. The formation of the PCTL assembly was easily achieved by dip-coating onto polyurethane (PU), one of the most widely used blood-contacting materials, in a mixed aqueous solution of LZM (1

mg/mL) and APS (2–10 mg/mL) at pH 5. Scanning electron microscopy (SEM) analysis revealed the presence of nanoscale particles on the modified substrates, confirming the successful formation of the PCTL assembly (Fig. 2a). X-ray photoelectron spectroscopy (XPS) analysis of PU after 12 h of dip-coating revealed the presence of C 1s, N 1s, O 1s and especially S 2p signals on the PCTL-modified surface, further indicating the successful constructing of the PCTL assemblies on the PU substrate (Fig. 2b). To gain a deeper understanding of the chemical components of the PCTL assemblies, peak fitting procedures were applied to the S 2p peaks in the XPS spectra. Two strong peaks located at 168.2 and 169.2 eV were observed and assigned to the R-SO<sub>2</sub>-O-S2p3 and R-SO<sub>2</sub>-O-S2p1, respectively. Additionally, a visible decrease in the intensity of shoulders at 163.5 eV and 164.7 eV was observed in the high-resolution S 2p spectrum of PCTL assemblies compared to native LZM. This implied that the disulfide bond of LZM was broken down and oxidized to sulfonate groups after treatment with APS (Fig. 2c). This estimate was further supported by Raman spectroscopy analysis of PCTL assemblies (Fig. 2d). The Raman spectra demonstrated a reduction in the intensity of the disulfide bond of LZM at 505 cm<sup>-1</sup> and the Cys bond of LZM at 755 cm<sup>-1</sup> with the addition of APS, indicating the oxidation activity of APS

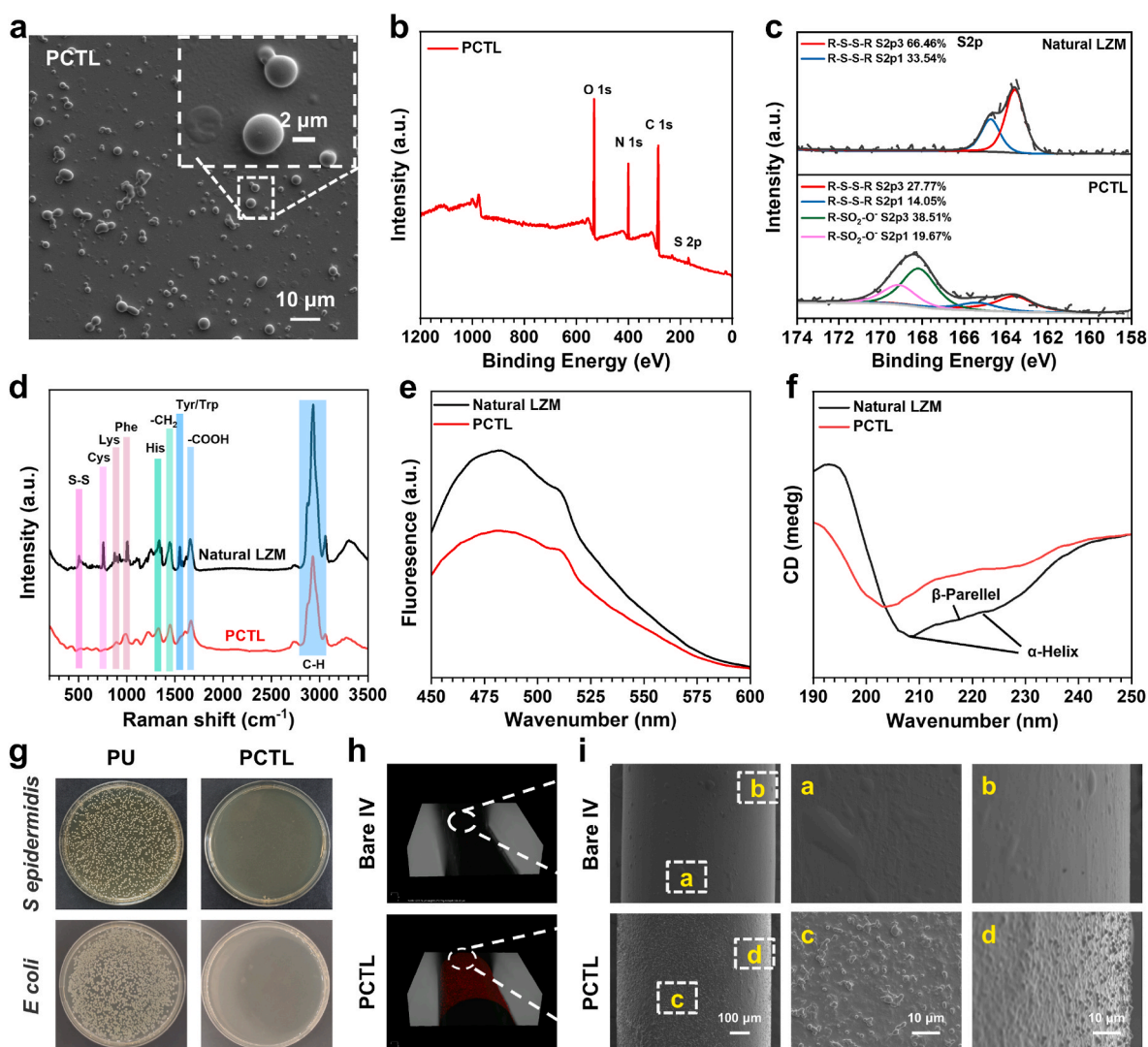


**Fig. 2.** Characterization of PCTL on polyurethane (PU) substrate. (a) SEM images of the PU substrate before and after modification by PCTL. (b) XPS characterization of PU before and after modification by PCTL. (c) High-resolution spectra of S2p. (d) Raman spectra of the PCTL and natural LZM. (e) The ANS fluorescence spectra of the natural LZM and PCTL. (f) Circular Dichroism (CD) spectra of PCTL and natural LZM. (g) Antibacterial rate of PCTL-armed PU that calculated from the number of colonies against *S. epidermidis* and *E. coli*. (h) Fluorescence images of the bare medical catheter and modified medical catheter substrates after labeled by NHS-FITC with red fluorescence. (i) SEM images of the bare medical catheter and modified medical catheter substrates.

towards the disulfide bond of Cys-Cys. Furthermore, the Raman spectra provided additional evidence of the presence of diverse functional groups on the surface of the PCTL coating, which included amino, carboxyl, hydroxy, sulfhydryl, amide, and hydrophobic carbon structures [44].

Disulfide bonds, which are formed between two cysteine residues in proteins by covalent bonds, play a critical role in their spatial structure and stability [45]. Disruption or reduction of disulfide bonds can expose amino acid residues and lead to protein conformational unfolding, which can have significant implications for protein function, interactions, and aggregation [46]. To monitor the exposure and aggregation of hydrophobic residues in LZM after treatment with APS, anilino-1-naphthalene sulfonate (ANS) was used as a fluorescent probe [47]. Upon addition of APS, the fluorescence intensity in the ANS and lysozyme mixture exhibited a rapid decrease. This observation indicated that the hydrophobicity of suspended protein colloids was weakened with the conformation transition proceeding after 4 h. This weakening can be attributed to the facilitation of PCTL aggregation through hydrophobic interactions among proteins, thereby reducing the exposure of hydrophobic residues in the system. (Fig. 2e). Far-UV circular dichroism (CD) was further carried out to investigate the secondary structural changes of LZM during the conformation transition process and probe the protein unfolding (Fig. 2f). The CD spectrum of the conformation transition buffer of LZM, revealed a change from the  $\alpha$ -helix peaks at 208 and 222 nm of native lysozyme to a single peak at 216 nm, indicating the significant increase in  $\beta$ -sheet structure in the PCTL. Additionally, the extent of  $\beta$ -sheet structure transformation in PCTL can be controlled by adjusting the concentration of APS. (Fig. S1). The three-dimensional structure of a protein is essential for its interaction with other molecules, such as substrates, enzymes, receptors, or DNA. Changes in the protein conformation can disrupt these interactions, leading to loss of biofunction. Therefore, our goal was to achieve the formation of a PCTL surface on the substrate while preserving the antimicrobial activity of PCTL. This was accomplished by modulating the optimal molar ratio of APS to LZM to induce partial LZM unfolding and facilitate heterogeneous nucleation and assembly. To evaluate the antibacterial efficacy of the optimized PCTL surface, we selected *Staphylococcus epidermidis* (*S. epidermidis*) and *Escherichia coli* (*E. coli*) as representative strains of Gram-positive and Gram-negative bacteria, respectively (Fig. 2g). Antibacterial experiment showed that PCTL surface exhibited significant inhibitory effects on bacterial growth, as verified by the antibacterial rates of 99.9% for *E. coli* and 99.9% for *S. epidermidis* (Fig. S2). These results confirmed the successful constructing of the PCTL surface with excellent antibacterial properties on the PU substrate.

One of the advantages of the proposed PCTL surface is that it is not dependent on specific substrate characteristics, allowing for its application on a wide range of common substrates with diverse geometries and applications. Moreover, the presence of diverse functional groups, especially amino groups, on the surface of the PCTL coating, provided the possibility for further secondary reaction to create a variety of ad-layers. We further demonstrate the applications of PCTL surfaces on commonly used biomedical devices, such as medical tubing. To further visualize the successful formation of PCTL surfaces on medical tubing, NHS-FITC was used. Briefly, NHS-FITC was incubated with the medical tubing deposited PCTL surfaces through carbon-diimide chemistry. Fluorescence microscopy images in Fig. 2h, the uniform and compact PCTL coatings deposited on medical tubing were clearly observed, further indicating the secondary reactivity of the  $-\text{NH}_2$  group on the PCTL. SEM analysis also confirmed the successful deposition of PCTL surfaces on medical tubing, as evidenced by the uniform distribution of nanoscale particles, which may be beneficial in creating a possible super-hydrophilic surface [48]. Overall, these results demonstrate the potential of PCTL for fabricating antibacterial surfaces on substrates with diverse geometries. Furthermore, a wide range of ad-layers can be achieved through subsequent secondary reactions to meet the

requirements of various application scenarios.

### 3.2. Fabrication and characterization of pMPC&PCTL

To enhance the long-term anti-thrombosis and antibiofilm capabilities of the PCTL assembly for blood-contacting devices, we drew inspiration from the extracellular membrane and grafted poly-2-methacryloyloxyethyl phosphorylcholine (pMPC) zwitterionic molecular brushes to armor the PCTL assembly. This created a super-hydrophilic armor with anti-adhesive properties for the PCTL assembly. The process involved tethering N-Hydroxysuccinimide acrylate (NAS) onto the PCTL-modified PU substrates or tubes through carbodiimide chemistry to introduce carbon-carbon double bond reactive sites (referred to as NAS-PCTL). Subsequently, the NAS-PCTL-modified PU was armored with a super-hydrophilic pMPC molecular brush using an MPC monomer solution catalysed by an inorganic peroxide initiation system (referred to as pMPC&PCTL). As shown Fig. 3a, various surfaces (PCTL, NAS-PCTL and pMPC&PCTL) was successfully formed on PU substrates, as evidenced by a slight blurring of school badge pattern. SEM analysis further confirmed the presence of nanoscale particles on the modified substrates even after grafting pMPC (Fig. 3b). To further visualize the successful formation of pMPC&PCTL surfaces on PU substrates, Rhodamine 6G (a fluorescent dye for pMPC) was used. The distinct point-like fluorescence signals observed on the surface of pMPC&PCTL, confirmed the successful grafting and polymerization of pMPC (Fig. 3c). We further conducted quantitative analysis of the distinct point-like fluorescence signals observed on the surface of pMPC&PCTL, showing that the signal density of pMPC polymer brushes on the surface was  $140.02 \pm 23.97$  count/cm<sup>2</sup>.

Reflection absorbance Fourier transform infrared (RA-FTIR) and X-ray photoelectron spectroscopy (XPS) analysis were conducted to assess the changes in the chemical structure and composition of the PCTL-modified PU before and after each grafting step. After NAS immobilization, the introduction of C=C peak by NAS in the FTIR spectra was nearly invisible. However, the appearance of the peaks at  $1724\text{ cm}^{-1}$  in the FTIR spectra indicated the successful grafting of NAS, as evidenced by the significant reduction in amino group density on the PCTL surface after NAS grafting (Fig. S3). The MPC grafting step introduced active-anchoring sites for MPC through the introduction of carbon-carbon double bond groups to the PCTL surface. The appearance of bands at  $1076\text{ cm}^{-1}$  (C-N<sup>+</sup>) and  $959\text{ cm}^{-1}$  (P-O-C) in the FTIR spectra, attributed to the MPC, suggested the successful grafting and polymerization of MPC (Fig. 3d). XPS analysis provided further confirmation of the successful surface engineering of NAS-PCTL and pMPC&PCTL. The reduction in sulfur (S) content and the nitrogen:carbon (N:C) atomic ratio of the NAS-PCTL confirmed the successful immobilization of NAS on the PCTL surface. Additionally, the appearance of phosphorus (P) element specific to MPC, further verified the introduction of pMPC on the NAS-PCTL surface (Fig. 3e and S4). Peak fitting procedures on the C 1s and O 1s peaks of the XPS spectra provided deeper insights into the chemical components of the functionalized surfaces. The appearance of a new peak at  $284.28\text{ eV}$  in the C 1s high-resolution spectra of the NAS-PCTL surface, suggested the introduction of carbon-carbon double bond groups by NAS. Moreover, the presence of C-N<sup>+</sup> peak in the C 1s high-resolution spectra of the pMPC&PCTL surface further suggested the successful grafting and polymerization of MPC on NAS-PCTL surface (Fig. 3f). The O 1s core-level spectrum of pMPC&PCTL further confirmed the successful formation of the pMPC&PCTL surface, as evidenced by the presence of P-O and P=O peaks (Fig. 3g). These results jointly verified the successful fabrication of the pMPC&PCTL surface.

The precise control of zwitterionic polymer brush thickness on a surface is crucial for achieving ultralow fouling and optimal antifouling performance [49]. Therefore, through optimizing the grafting and polymerization conditions (Fig. S5), we successfully obtained an pMPC zwitterionic polymer brush with a thickness exceeding 50 nm on surface (Fig. 3h). This imparted super-hydrophilic properties to the

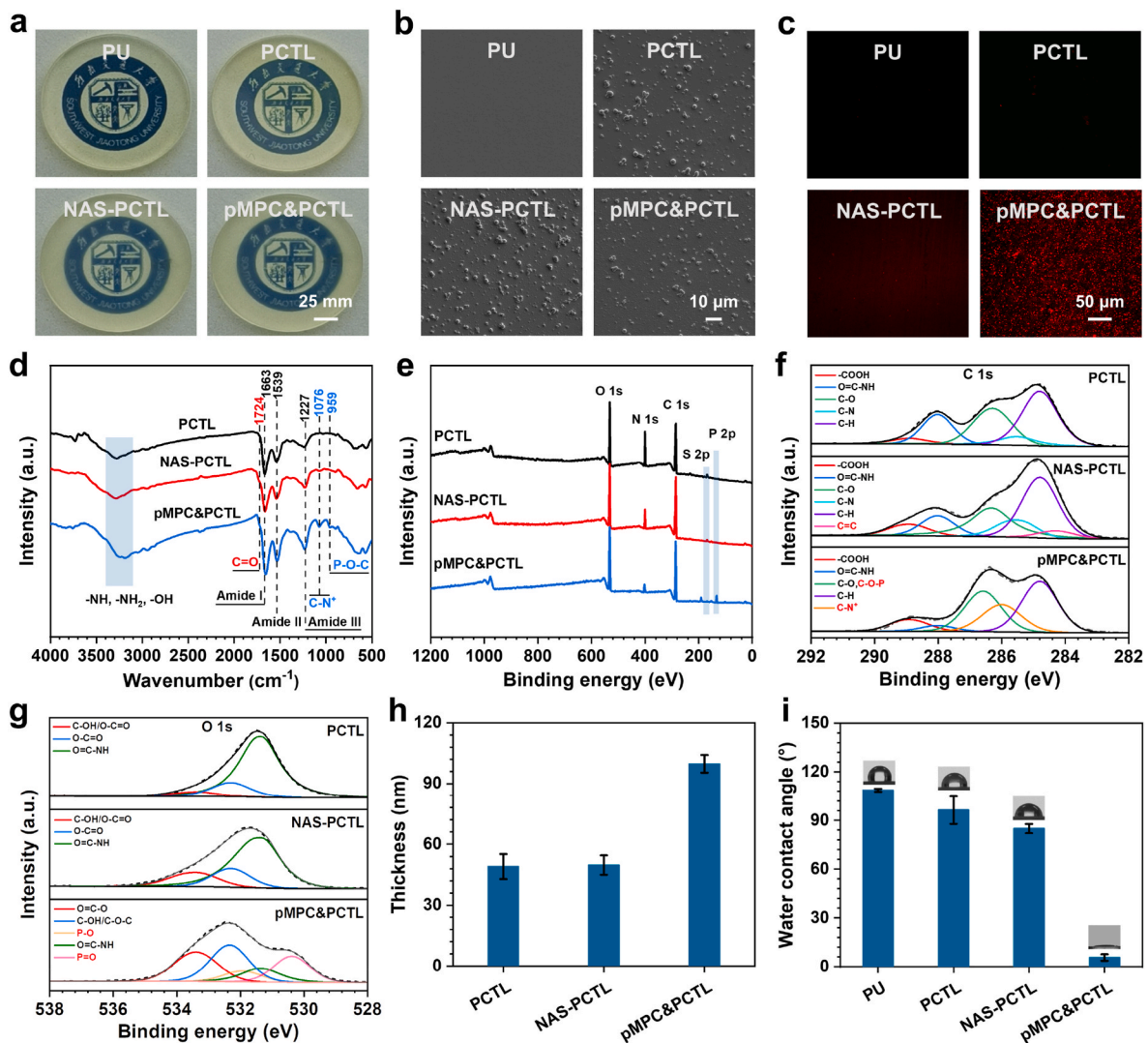


**Fig. 3.** Characterization of pMPC&PCTL on polyurethane (PU) substrate. (a) Photographs of and SEM images (b) the PU substrates before and after modification by PCTL, NAS-PCTL and pMPC&PCTL. (c) Fluorescence images of the bare PU and modified PU substrates after labeling by Rhodamine 6G with red fluorescence (a fluorescent staining for MPC). (d) FTIR spectra of PCTL surface after grafting with NAS and MPC. (e) XPS characterization of PU before and after modification by PCTL, NAS-PCTL and pMPC&PCTL. (f–g) High-resolution spectra of C1s (f) and O1s (g). (h) Thickness evolution of pMPC&PCTL on Si as measured by ellipsometer (EP). (i) Variations in surface wettability on PU substrates before and after modification by PCTL, NAS-PCTL and pMPC&PCTL.

pMPC&PCTL surface, with a water contact angle (WCA) of  $5.72 \pm 2^\circ$  (Fig. 3i). Altering the surface wettability of materials can modify the adhesion behaviour of substances on the material surface [50]. This super-hydrophilic armor can endow the PCTL assembly with excellent anti-adhesion capacity.

### 3.3. Anti-bacterial property

Infection poses a significant risk associated with indwelling medical devices and extracorporeal circuits, potentially leading to mortality in clinical [51]. To evaluate the antibacterial properties of the pMPC&PCTL surface, *S. epidermidis* and *E. coli* was selected as representative strains of Gram-positive and Gram-negative bacteria, respectively, commonly involved in biofilm-associated infections related to biomaterials.

The initial adhesion of bacteria is a crucial step in biofilm formation on solid surfaces [52]. Therefore, an ideal antibacterial surface should effectively reduce the quantity and viability of attached bacteria during the early stages of adhesion. To test the short-term (12 h) antibacterial properties the pMPC&PCTL surface, colony counting assay and SEM

assay were carried out (Fig. 4a–b and S6–S7). As shown in Fig. 4a, a substantial number of bacteria attached on the pristine PU surface. These attached bacteria displayed typical shapes with well-defined edges and intact membranes, indicating the lack of bactericidal activity associated with the PU substrate. In contrast, the PCTL-coated PU surface exhibited significant inhibitory effects on bacterial growth, with antibacterial rates of 99% for *E. coli* and 99% for *S. epidermidis*. SEM analysis revealed bacterial membrane rupture in the PCTL group, which may be attribute to the antibacterial ability of LZM to penetrate and destroy the bacterial membrane [53], thus suggesting that the antibacterial activity of PCTL was well maintained. Similar inhibitory effects on bacteria were observed for the NAS-PCTL and pMPC&PCTL groups, demonstrating antibacterial rates of nearly 99.9% against *E. coli* and *S. epidermidis*. These findings indicated that the introduction of NAS and pMPC did not affect the overall antibacterial properties of PCTL surface, which is further supported by liquid media technique (Fig. S6). Furthermore, the pMPC&PCTL surface exhibited a significant reduction in bacterial attachment compared to other groups (Fig. S7). In fact, bacteria achieve adhesion to material surfaces through the secretion of adhesins, owing to the presence of adhesive moieties within the

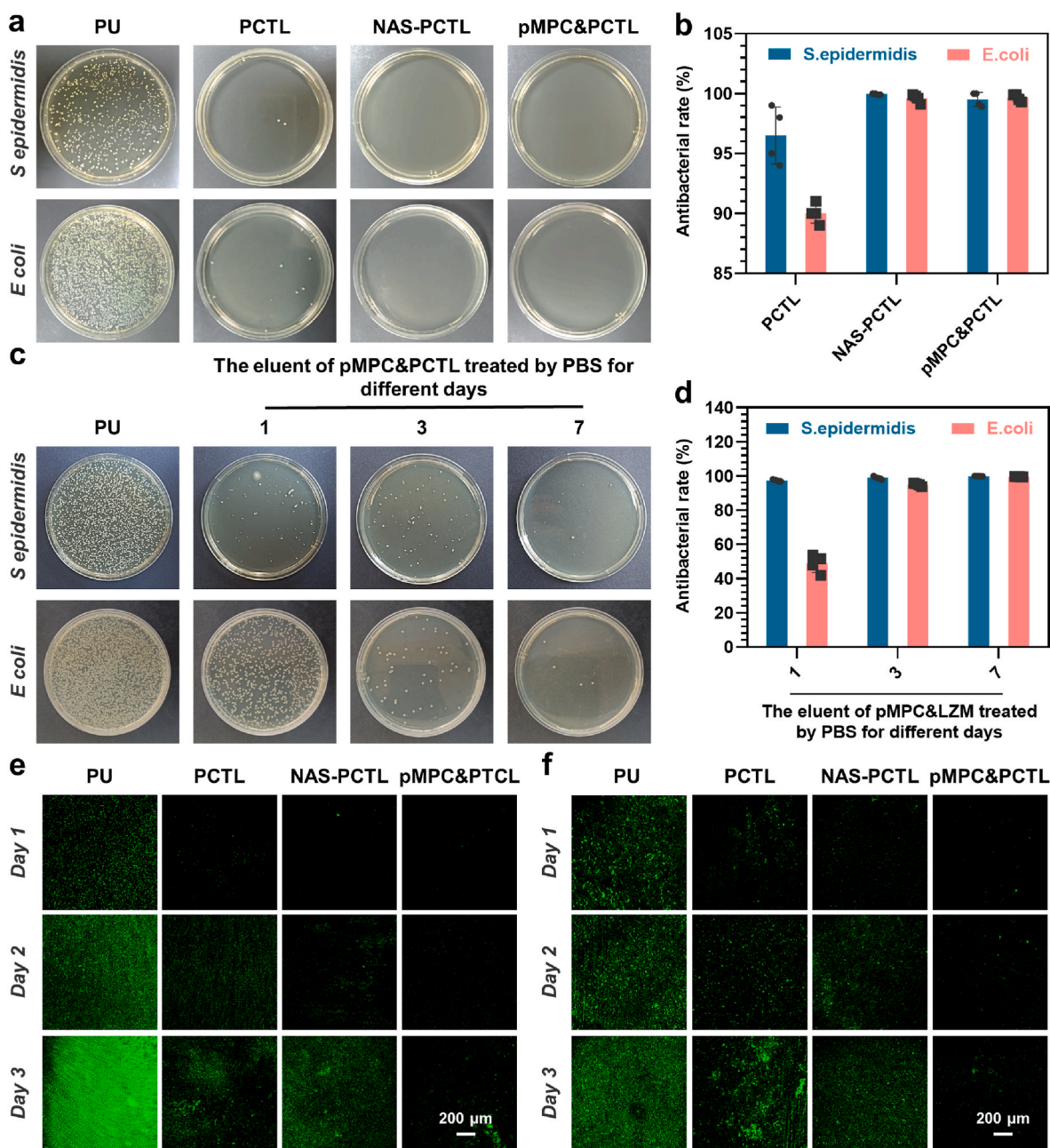


**Fig. 4.** Anti-bacterial property. (a) Typical *S. epidermidis* and *E. coli* colonies after 24 h incubation on the bare and modified PU plates, respectively. (b) Antibacterial rate of modified PU that calculated from the number of colonies against *S. epidermidis* and *E. coli*. (c) Typical *S. epidermidis* and *E. coli* colonies after 24 h incubation with the eluent of pMPC&PCTL treated by PBS for different days, respectively. (d) Antibacterial rate of the eluent of pMPC&PCTL that calculated from the number of colonies against *S. epidermidis* and *E. coli*. (e–f) Fluorescence microscopy images of *S. epidermidis* (e) and *E. coli* (f) biofilms formed on different samples at different periods of time, respectively. Data presented as mean  $\pm$  SD ( $n = 4$ ) and analyzed using a one-way ANOVA.

bacterial adhesins, such as various charged and hydrophobic groups [54]. Therefore, such anti-adhesion properties to bacteria could be attributed to the super-hydrophilic pMPC zwitterionic molecular brush, which facilitated the binding of water molecules through hydrogen bonds and electrostatic action, forming a hydration armor to prevent bacterial adhesins adhesion [55]. Taken together, these results demonstrated that all the modified surfaces, compared to pristine PU, exhibited favorable short-term antibacterial activity by effectively preventing the initial bacterial attachment and killing bacteria adhered on the surface.

In our “Armored-Tank” design, the pMPC&PCTL surface passively prevent bacterial adhesion through the hydration armor formed by pMPC zwitterionic molecular brush. Additionally, such “Armored-Tank” actively released LZM, effectively killing both Gram-positive and Gram-

negative bacterial as a supplement to the lacking bactericidal functions of passive outer armor. To further verify the feasibility of our design, antibacterial experiments were performed using the eluent obtained from the pMPC&PCTL surface. Briefly, the eluent obtained from the pMPC&PCTL surface after treatment with PBS for different durations (1, 3 and 7 days), was collected to assess its effect on bacterial growth and viability (Fig. 4c and d). The results of the antibacterial experiments revealed a time-dependent antibacterial performance of the elution solution. As the immersion time increased, the antimicrobial efficacy of the elution solution also increased, eventually reaching a high level of 99%. This may be attributed to the concentration of LZM in the elution solution, which increased with longer treatment times. This judgement was further confirmed by quantitative analysis of LZM concentration in

the eluent, using ultraviolet spectrophotometer (UV) (Fig. S8). The monitoring of LZM concentration in the elution solution revealed a time-dependent relationship, wherein the concentration of LZM increased as the immersion time was prolonged. These results indicated that the release of LZM from the surface was time-dependent with a gradual accumulation of LZM in the eluent over time, which is likely contributed to the enhanced antibacterial activity observed in the elution solution with longer immersion times.

Encouraged by the promising short-term antibacterial property of pMPC&PCTL surface, we conducted further investigations to evaluate its long-term antibiofilm performance, which was still a more challenging aspect for many conventional antibacterial surfaces. To evaluate the long-term antibiofilm performance of pMPC&PCTL surface, all samples were incubated in a bacterial suspension for 6 h. Subsequently, the samples were gently rinsed and transferred to new wells with nutrient medium to support biofilm growth. The biofilms formed on the samples were then characterized at specific time intervals (1, 2 and 3 days) for analysis and evaluation. First, the bacteria within biofilms were visualized by staining them with SYTO 9 (Fig. 4e and f). In contrast to the sparsely distributed bacteria observed in the short-term results, the PU group exhibited bacterial aggregations after 1 day of culture in the nutrient medium, indicating the rapid formation of a biofilm. As the culture time extended, the biofilm became denser and eventually covered the entire surface. Conversely, on Day 1, few bacterial aggregations were observed on the PCTL, NAS-PCTL, and pMPC&PCTL surfaces, potentially due to their inherent antibacterial activities. However, after incubation for 2 days, the antibacterial efficacy of the PCTL and NAS-PCTL surface declined, as evidenced by an increase in both the area and intensity of the fluorescence signal, suggesting the formation of biofilm on these surfaces. Notably, the pMPC&PCTL group exhibited a

remarkable ability to inhibit the formation of biofilm for up to 3 days, indicating the long-term biofilm-inhibition properties of pMPC&PCTL surface. However, as a biological material, we need to consider its ability to exhibit antibacterial properties while ensuring the absence of toxicity towards tissues. Therefore, we further verified the cytocompatibility of pMPC&PCTL using L929 mouse fibroblast cells according to the American Society for Testing Materials (ASTM) F813 standard. The CCK-8 assay demonstrated that pMPC&PCTL did not cause cytotoxicity or affect the growth and proliferation of L929 cells (Fig. S9), suggesting the cytocompatibility of the pMPC&PCTL.

Overall, these results indicated that the bactericidal surfaces (e.g., PCTL and NAS-PCTL) exhibited a delay in biofilm formation during the initial stages, whereas were not effective in preventing biofilm formation over an extended period. On the other hand, the germicidal surface may experience a reduction in bactericidal activity due to the accumulation of dead bacteria and their debris, potentially covering the actively germicidal groups. In contrast, the pMPC&PCTL surface combined passive prevention of bacterial adhesion through the hydration armor formed by the pMPC molecular brush with active “fired” LZM for bacterial eradication, thereby endowing blood-contacting devices with excellent long-term antibacterial ability.

### 3.4. *In vitro* blood compatibility tests

Foreign materials that come into contact with blood can trigger a series of reactions, such as blood protein adsorption, complement system and coagulation cascade activation, which ultimately lead to thrombus formation. Two major contributors to thrombus formation on blood-contacting implants are the adsorption and activation of fibrinogen (Fg) and the adhesion and activation of platelets [37].

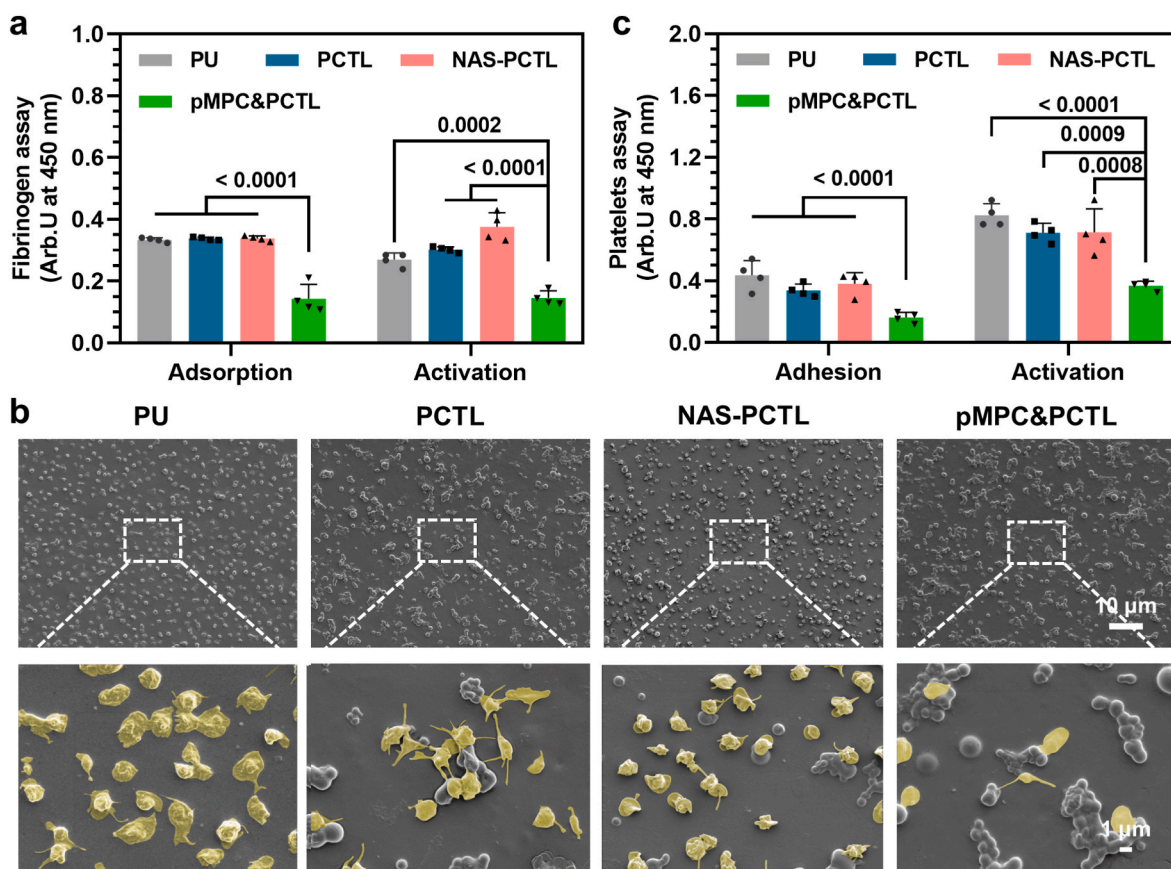


**Fig. 5.** *In vitro* blood compatibility evaluation. (a) Adsorption and activation of the adhered fibrinogen on bare and modified PU. (b) SEM images of the adhered platelets on bare and modified PU (all scale bars from the same raw are 10 or 1  $\mu$ m). (c) Adhesion and activation of the adhered platelets on bare and modified PU. Data presented as mean  $\pm$  SD ( $n = 4$ ) and analyzed using a one-way ANOVA.

Upon contact with blood, Fg, a critical serum protein, quickly adsorbs onto the surface of foreign materials. The adsorption and activation of Fg play a critical role in coagulation processes and bacterial adhesion, significantly influencing the subsequent performance of blood-contacting devices. As shown in Fig. 5a, both PCTL and NAS-PCTL surfaces did not exhibit significant alterations in the behaviour of fibrinogen compared to the bare polyurethane (PU) surface. However, the grafting of pMPC led to a significant reduction in the adsorption and activation of fibrinogen, implying a zone defensive effect of pMPC molecular brush on fibrinogen. This assessment was further supported by evaluating the adhesion of fluorescently-labeled fibrinogen on different samples (Figs. S10 and S11). The presence of the pMPC zwitterionic molecular brush created a hydration armor that limited the interaction between fibrinogen and the material surface, resulting in decreased adsorption and subsequent activation of fibrinogen. Furthermore, we

further investigated the antiplatelet property of the pMPC&PCTL surfaces *in vitro*. To further evaluate the effects on platelet adhesion and activation, scanning electron microscopy (SEM) was employed to analyze the surfaces after exposure to platelet-rich plasma (PRP) for 30 min (Fig. 5b). A substantial number of platelets adhered to the PU groups, exhibiting a high degree of activation and aggregation. Compared to PU groups, the PCTL and NAS-PCTL surfaces showed a slight decrease of platelet adhesion and activation, possibly due to the excellent biocompatibility of the PCTL coating. In contrast, the pMPC&PCTL group substantially inhibited adhesion and activation of platelets with an inactive spherical state, indicating the excellent anti-platelets properties of the hydration armor formed by pMPC molecular brush. Quantitative of the level of LDH and P-Selectin of the platelets adhere onto different sample groups further confirmed that the significant reduction in thrombosis formation of the pMPC&PCTL groups compared to the other

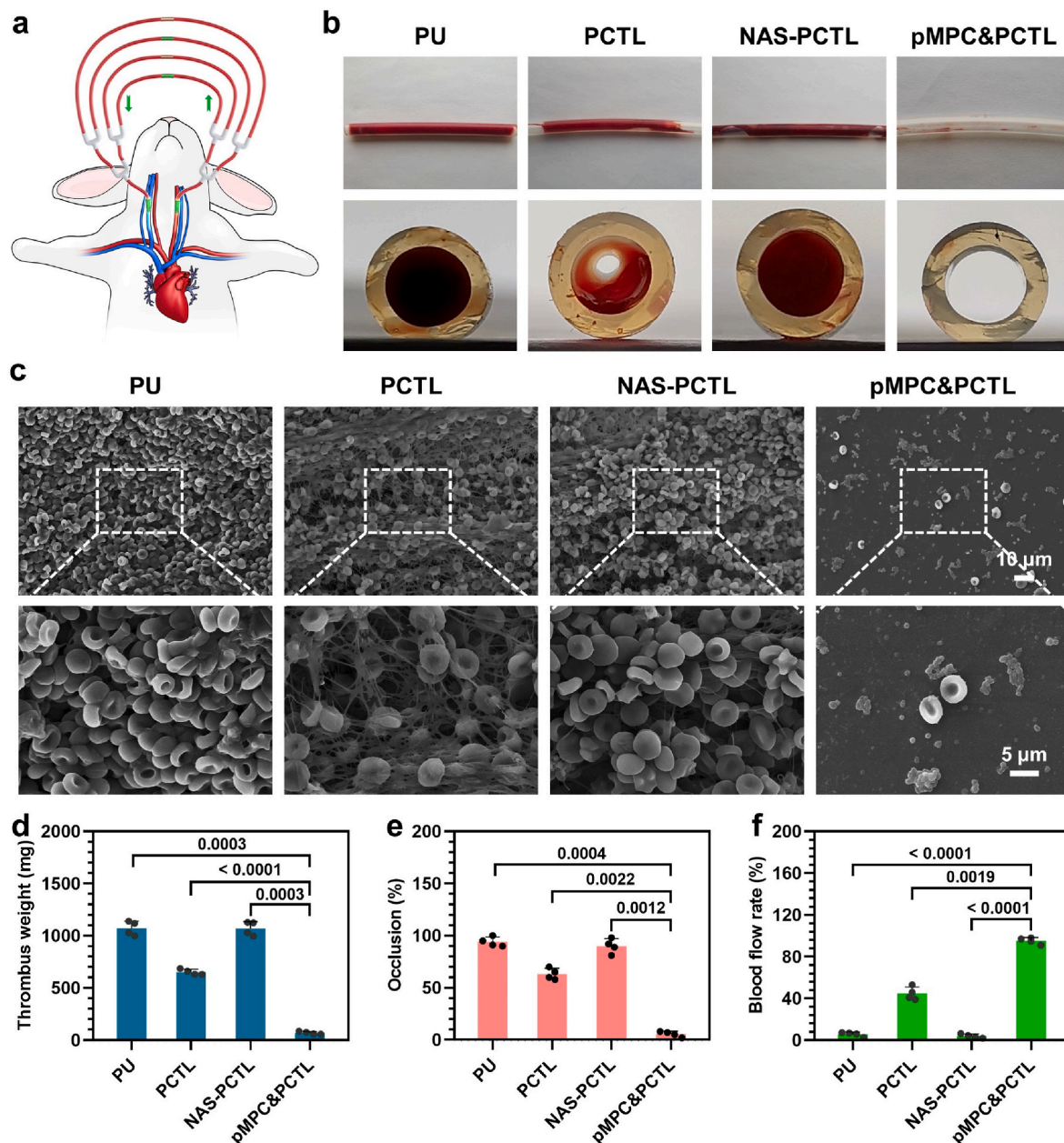


Fig. 6. Ex vivo hemocompatibility of the pMPC&PCTL surfaces. (a) Schematic illustration of arteriovenous (AV) shunt model connected to the rabbit. (b) Photographs of side (top) and cross-section (bottom) view of the bare and modified PU tubes after blood circulation. (c) Lumen surface morphology of each sample after blood circulation characterized by SEM. (d) thrombus weight, (e) occlusion and (f) Blood flow rate of bare and modified PU tubes after blood circulation for 3 h. Data presented as mean  $\pm$  SD ( $n = 4$ ) and analyzed using a one-way ANOVA.

groups (Fig. 5c). Additionally, haemolysis experiments were conducted to evaluate the safety of pMPC&PCTL surface before use *in vivo* as a blood-contacting material. The haemolysis rate of all groups was less than 2%, indicating that the pMPC&PCTL surface meet the clinical requirements (Fig. S12). Taken together, these results demonstrated that the surface engineering of PU with pMPC&PCTL provided an anti-adhesion hydration armor that remarkably suppressed the adhesion and activation of fibrinogen and platelets, thereby reducing thrombogenicity *in vitro*.

### 3.5. Ex vivo antithrombogenic properties

To further simulate a clinical application, an *ex vivo* catheter blood extracorporeal circuit experiment was conducted [37]. Commercially used PU tubing with different surface treatments was assembled with a

commercially available medical catheter and connected to a rabbit arteriovenous shunt circuit. (Fig. 6a).

After *ex vivo* flow circulation for 2 h without any systemic heparin anticoagulation, the circuits of pMPC&PCTL surface exhibited significant reductions in occlusive thrombosis compared to the control groups (Fig. 6b). Remarkably, a minimal thrombus formation on the pMPC&PCTL groups was observed, while the control groups (PU, PCTL and NAS-PCTL) exhibited significant thrombus formation. SEM analysis provided further confirmation that the presence of pMPC molecular brush in the groups effectively prevented thrombus formation. However, the blood-contact surfaces of the bare PU, PCTL and NAS-PCTL-modified tubing displayed severe thrombus formation characterized by densely interconnected polymeric fibrin networks, red blood cells and activated platelets (Fig. 6c). Quantitative analysis of these results further demonstrated a substantial decrease in thrombosis formation in the

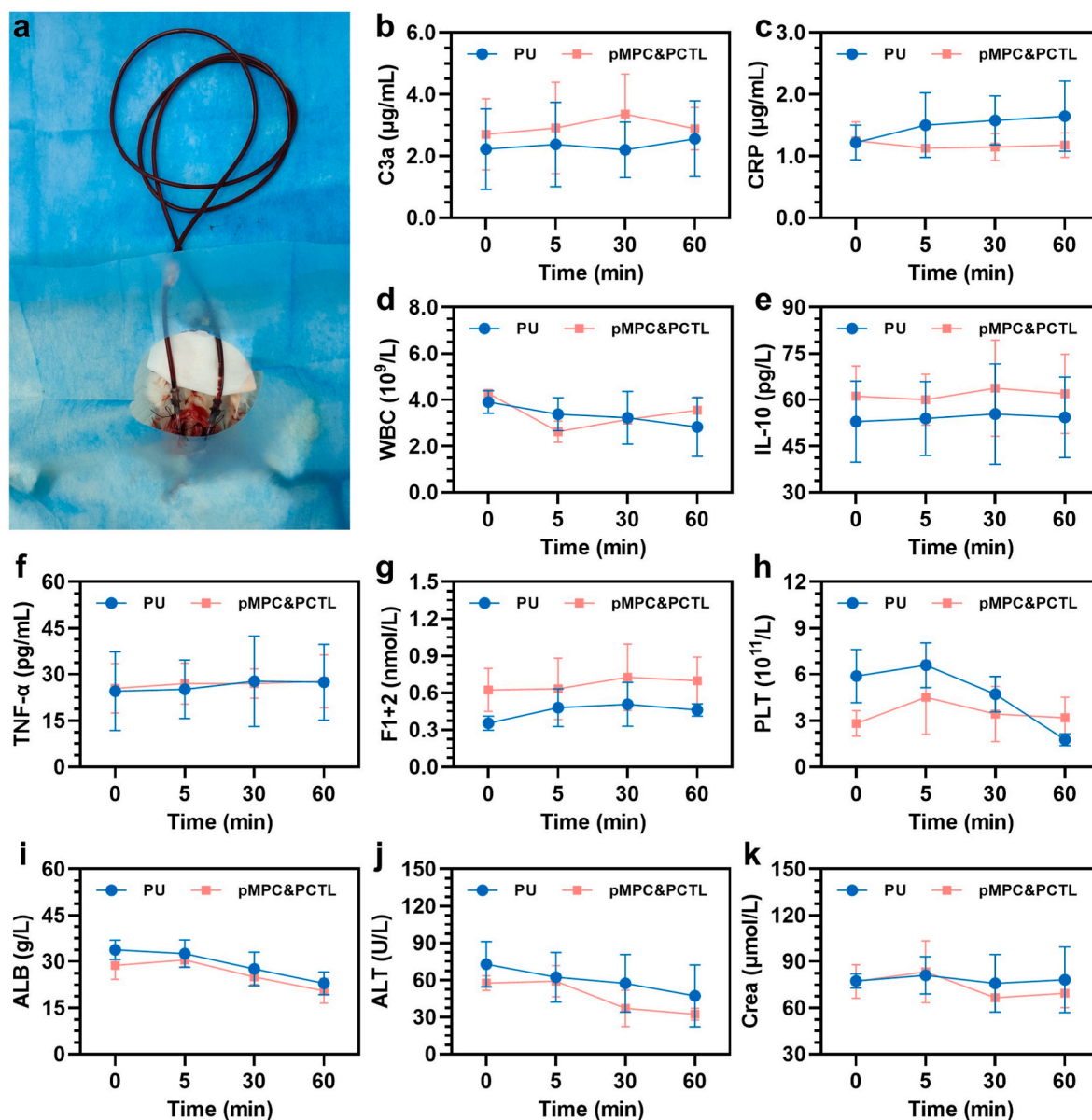


Fig. 7. Blood analysis by *ex vivo* blood circulation. (a) Circulation model on rabbit for blood analysis. Blood parameters including (b) C3a (C3 cleavage fragment, indicating the classic or alternative way to activate the complement system), (c) c-reactive protein (CRP), (d) white blood cells (WBC), (e) IL-10 (a recognized inflammatory and immunosuppressor), (f) tumor necrosis factor alpha (TNF- $\alpha$ ), (g) F1+2 (an integral marker for the prothrombin activation), (h) the number of platelets (PLT), (i) Serum albumin (ALB), (j) the liver enzyme alanine aminotransferase (ALT) and (k) the kidney parameter serum creatinine (Scr) were measured to assess the hemocompatibility and liver/kidney safety following exposure of both bare and pMPC&PCTL-grafted catheters to circulating pRabbit blood. Data are presented as mean  $\pm$  SD ( $n = 4$ ).

pMPC&PCTL group compared to the other groups, as evidenced by the evaluation of thrombus weight, occlusion rates and blood flow rates of the circuits (Fig. 6d–f). Specifically, the total thrombus weight in the pMPC&PCTL circuits was reduced by 15.4-fold, 9.37-fold, and 15.39-fold as compared with bare PU, PCTL and NAS-PCTL group, respectively (Fig. 6d). In addition, the occlusion rates within the circuits were assessed by calculating the percentage of lumen area occlusion using computerized image analysis. Compared to the bare, PCTL and NAS-PCTL groups, the pMPC&PCTL-modified circuit exhibited a significant reduction in thrombotic occlusion, with an approximate occlusion rate of 8% (Fig. 6e). Consistent with the observed reduction in thrombotic occlusion, the blood flow rates in the pMPC&PCTL-modified circuit also demonstrated a significant improvement (Fig. 6f). These results are consistent with the previously described *in vitro* anti-thrombogenic property of the pMPC&PCTL surface.

### 3.6. Blood biochemical analysis

To ensure the safety of long-term or large-area blood-contacting biomedical devices, such as central venous catheters or cardiopulmonary bypass systems, a comprehensive assessment of their impact on blood composition as well as liver and kidney functions must be conducted in a systematic manner. Give the difference of total blood volume between rabbit and human (~200 mL for mature white rabbit and ~4000 mL for adult human), a bare PU or pMPC&PCTL-modified tube, measuring 1.6 m in length and having an inner diameter of 3 mm, was selected to simulate the clinical application, and then inserted into the jugular AV shunt of a rabbit [56] (Fig. 7a). At specific time intervals of 0, 5, 30, and 60 min of circulation, blood samples were collected to assess physiological and biochemical parameters, such as coagulation, inflammatory response, and organ functions.

Upon implantation of a device *in vivo*, it promptly triggers an immune system response, leading to an inflammatory reaction. After circulation, the pro-inflammatory parameters of all groups showed no significant changes: the levels of C3a (a cleavage fragment of C3 that indicated the activation of the complement system through the classical or alternative pathways, Fig. 7b), c-reactive protein (an acute phase protein used to measure acute inflammation, Fig. 7c), white blood cell count (WBC) (Fig. 7d), IL-10 (an immunosuppressive cytokine with inflammatory properties, Fig. 7e) and the expression of tumor necrosis factor alpha (TNF- $\alpha$ ) (a major cytokine associated with acute inflammation, Fig. 7f). These results jointly indicated that none of the groups exhibited a pro-inflammatory tendency. The pro-inflammatory indicators in the pMPC&PCTL surface group exhibited consistent results with those of the bare PU group used in clinical, which suggested that the pMPC&PCTL surface did not enhance the inflammatory response of the material. In the coagulation evaluation, all sample groups did not exhibit a propensity for blood clotting after prolonged exposure to blood, as evidenced by an increase in the levels of F1+2, an integral marker for prothrombin activation (Fig. 7g). Additionally, there was no significant impact on the platelet count (PLT) in the control group compared to the pMPC&PCTL group, possibly due to the occurrence of coagulation (Fig. 7h). To investigate potential adverse reactions of the material and coating on organs and tissues, the concentrations of alanine aminotransferase (ALT), a liver enzyme, and serum creatinine (Scr), a kidney parameter, were measured. The results demonstrated that both the PU and pMPC&PCTL groups showed no significant of organ and tissue toxicity during the circulation period (Fig. 7j–k). Moreover, there was no significant difference observed between the bare and coated PU catheters, confirming their biosafety.

### 3.7. Durability of antifouling properties of pMPC&PCTL surface

Ensuring the stability of functional coatings is critical for the successful clinical use of biomedical devices, particularly for indwelling needles or CVCs, that required potent resistance to infection and

thrombosis is essential for at least 15 days. To evaluate the durability of the antibacterial and anti-thrombogenic effects of the pMPC&PCTL surface for long-term implanted blood-contacting devices, such as central venous catheters, the samples were immersed in phosphate-buffered saline (PBS) for various durations. XPS analysis revealed the presence of pMPC on the surface ever after 15 days of immersion, as indicated by the relatively unchanged content of P element. However, the absence of P element after immersion of 30 days, indicated complete degradation of the pMPC hydration armor (Fig. 8a). Similarly, the film thickness remained at 37 nm after 30 days of immersion, compared to its initial thickness of 101 nm (Fig. 8b). Considering that the thickness of LZM coating was 49 nm, it can be inferred that the pMPC hydration armor had completely degraded after 30 days of immersion, resulting in the loss of the anti-adhesion function. In contrast, the residual pMPC hydration armor after immersion for 15 days was still 21 nm. Remarkably, after 7 days of immersion, the water contact angle of the pMPC&PCTL was less than 20°, and remained around 30° even after 15 days of immersion (Fig. 8c). These results suggested that the pMPC&PCTL surface still possessed antifouling properties even after 15 days of immersion. Furthermore, the pMPC&PCTL surface may maintain its antibacterial properties even after 30 days of immersion, due to the presence of the PCTL layer.

To evaluate the long-term durability of the pMPC&PCTL-modified PU under continuous exposure to PBS for 30 days, a biofouling test was conducted. Despite the extended immersion for 30 days, the coating exhibited remarkable antibacterial properties, as evidenced by the inhibition of 80% bacterial growth for both *E. coli* and *S. epidermidis* (Fig. 8d and e). To assess the long-term stability of the antithrombotic properties, an *ex vivo* circulation experiment was conducted on the pMPC&PCTL-modified tubes that had been exposed to PBS for 7, 15 and 30 days (Fig. 8f–i). After 2 h of circulation, the bare PU tube exhibited almost complete occlusion, whereas the pMPC&LZM-coated circuits after exposed to PBS for 0, 7 and 15 days, showed only minimal detectable occlusion 4.13%, 4.25% and 12.25%, respectively. However, after 30 days of immersion, the pMPC&PCTL-coated circuits lost their anti-adhesive performance, resulting in severe blood clot formation and nearly complete occlusion within 2 h of circulation. The pMPC molecular brush was responsible for the passive prevention of bacterial adhesion by creating a hydration armor that resisted protein and cell adhesion. However, the degradation of the pMPC polymer brushes could compromise their anti-adhesive properties over time, allowing for the adhesion of blood components and subsequent clot formation. (Fig. 8g). Quantitative analysis of the thrombi formed in the circuits showed a significant reduction in thrombus weight in the pMPC&PCTL-modified circuits after PBS treatment for 0, 7, and 15 days compared to the bare PU circuit. Specifically, the thrombus weight decreased from  $635.6 \pm 79.36$  mg in the bare PU circuit to  $69.52 \pm 13.19$  mg,  $50.25 \pm 13.25$  mg, and  $174.5 \pm 27.37$  mg in the pMPC&PCTL-modified circuits after PBS treatment for 0, 7, and 15 days, respectively (Fig. 8h). The minimal increase in thrombus weight observed after 15 days of PBS treatment indicated the sustained antithrombotic functionality of the pMPC&PCTL surface. Importantly, the blood flow rate of the pMPC&PCTL-modified tubing remained nearly constant even after 15 days of PBS treatment (Fig. 8i), suggesting the potential application of the pMPC&PCTL surface in long-term implanted or interventional blood-contacting devices, where maintaining stable blood flow is crucial.

## 4. Conclusion

In summary, we develop here a zwitterionic polymers-armed amyloid-like protein surface engineering strategy to create multifunctional anti-biofouling coating onto blood-contacting devices by highly integrated active attack and zone defense designs. To enhance the antimicrobial activity, the PCTL assembly was decorated on devices through oxidant-mediated partially conformation transition process. The super-hydrophilic pMPC zwitterionic molecular brush was then applied to

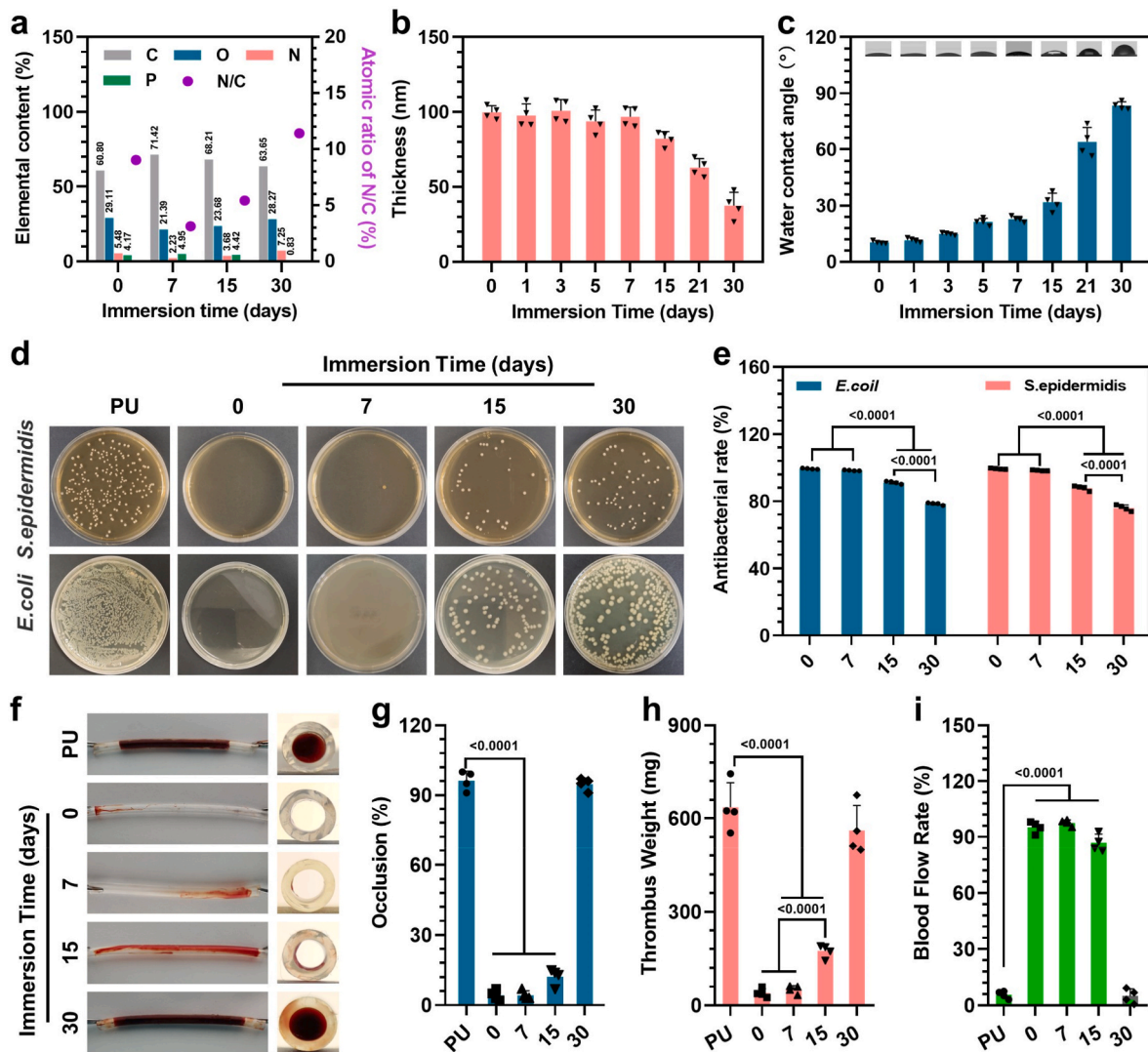


**Fig. 8.** Durability of antifouling properties of pMPC&PCTL surface. (a) Surface chemical composition of pMPC&PCTL surface on PU substrates after exposure to PBS with different days. The solution was replaced every 72 h. (b) Thickness of pMPC&PCTL surface on PU substrates after exposure to PBS with different days. The solution was replaced every 72 h. (c) Variations of pMPC&PCTL surface wettability on PU substrates after exposure to PBS with different days. The solution was replaced every 72 h. (d) Representative colonization of *S. epidermidis* and *E. coli* on bare and pMPC&PCTL-modified PU before and after treatments by PBS for different days. The solution was replaced every 72 h. (e) Antibacterial rates, calculated from the results of (d). (f) Photographs of side and cross-sectional of the unmodified and pMPC&PCTL-modified circuits before and after treatments by PBS for different day. The solution was replaced every 72 h. (g) occlusion rates, thrombus weight (h) and blood flow rates (i) of different circuits at the end of circulation experiments.

armor PCTL assembly through carbodiimide chemistry and free radical polymerization. This “Armored-tank” strategy endows medical devices with durable synergistic effects, against fibrinogen and platelet adhesion, as well as antimicrobial properties *in vitro*. Moreover, it effectively prevents thrombogenesis in rabbit blood circulation *ex vivo* without anticoagulation. Therefore, we envision that the “armored-tank” strategy is a promising candidate to prevent thrombotic occlusion and biofouling of blood-contacting medical devices.

#### Data availability statement

The data that support the findings of this study are available from the corresponding author upon reasonable request.

#### CRediT authorship contribution statement

**Xiaohui Mou:** Investigation, Methodology, Validation, Data curation. **Wan Miao:** Methodology, Data curation. **Wentai Zhang:**

Methodology. **Wenxuan Wang:** Methodology, Data curation. **Qing Ma:** Animal model construction. **Zeyu Du:** Animal model construction. **Xin Li:** Manuscript writing suggestions. **Nan Huang:** Project administration, Funding acquisition. **Zhilu Yang:** Supervision, Project administration, Funding acquisition, Writing – review & editing.

#### Declaration of generative AI and AI-assisted technologies in the writing process

During the preparation of this work the author used ChatGPT 3.5 in order to polish the language of the article. After using this ChatGPT 3.5, the author(s) reviewed and edited the content as needed and take(s) full responsibility for the content of the publication.

#### Declaration of competing interest

Prof. Zhilu Yang is an editorial board member for Bioactive Materials and was not involved in the editorial review or the decision to publish

this article. All authors declare that there are no competing interests.

## Acknowledgments

This work was supported by the National Natural Science Foundation of China (Project 82202325, 82072072, 32171326, 32261160372), the Guang Dong Basic and Applied Basic Research Foundation (2022B1515130010, 2021A1515111035), and China Postdoctoral Science Foundation (2022M721524).

## Appendix A. Supplementary data

Supplementary data to this article can be found online at <https://doi.org/10.1016/j.bioactmat.2023.09.003>.

## References

- [1] T.J. Vachharajani, J.J. Talierno, E.J. Anvari, New devices and technologies for hemodialysis vascular access: a review, *Am. J. Kidney Dis.* 78 (1) (2021) 116–124, <https://doi.org/10.1053/j.ajkd.2020.11.027>.
- [2] T. Matsuda, Device-directed therapeutic drug delivery systems, *J. Contr. Release* 78 (1–3) (2002) 125–131, [https://doi.org/10.1016/S0168-3659\(01\)00493-X](https://doi.org/10.1016/S0168-3659(01)00493-X).
- [3] I.H. Jaffer, J.C. Fredenburgh, J. Hirsh, J.I. Weitz, Haemostasis, Medical device-induced thrombosis: what causes it and how can we prevent it? *J. Thromb. Haemostasis* 13 (S1) (2015) S72–S81, <https://doi.org/10.1111/jth.12961>.
- [4] J.I. Shen, A.A. Mitani, T.I. Chang, W.C.J.N. Winkelmayer, dialysis, transplantation: official publication of the European Dialysis, T.A.-E.R. Association, Use Safe. Heparin-free Maintenance. *Hemodial. USA* 28 (6) (2013) 1589–1602, <https://doi.org/10.1093/ndt/gft067>.
- [5] Daniel C. Leslie, Anna Waterhouse, Julia B Berthet, Thomas M. Valentin, A bioinspired omniphobic surface coating on medical devices prevents thrombosis and biofouling, *Nat. Biotechnol.* 32 (2014) 1134–1140, <https://doi.org/10.1038/nbt.3020>.
- [6] M. Gorbet, C. Sperling, M.F. Maitz, C.A. Siedleck, M.V. Sefton, The blood compatibility challenge Part 3: material associated activation of blood cascades and cells, *Acta Biomater.* 94 (2019) 25–32, <https://doi.org/10.1016/j.actbio.2019.06.020>.
- [7] L. Song, J.J. Henry, Nonthrombogenic approaches to cardiovascular bioengineering, *Annu. Rev. Biomed. Eng.* 13 (1) (2011) 451–475, <https://doi.org/10.1146/annurev-bioeng-071910-124733>.
- [8] R.C.M. Jr, MRSA: the first half century, *J. Antimicrob. Chemother.* 67 (1) (2012) 4–11, <https://doi.org/10.1093/jac/dkr437>.
- [9] P.J. Pronovost, C.A. Goeschel, E. Colantuoni, S. Watson, L.H. Lubomski, S.M. Berenholtz, D.A. Thompson, D.J. Sinopoli, S. Cosgrove, J.B. Sexton, Sustaining reductions in catheter related bloodstream infections in Michigan intensive care units: observational study, *BMJ* 340 (2010) 462, <https://doi.org/10.1136/bmj.c309>, 462.
- [10] J.J.H. Badger, L.T.J.o. Acute, C. Care, Long peripheral catheters for deep arm vein venous access: a systematic review of complications, *Heart Lung* 48 (3) (2019) 222–225, <https://doi.org/10.1016/j.hrtlng.2019.01.002>.
- [11] R.E. Cronin, R.F. Reilly, Unfractionated heparin for hemodialysis: still the best option, *Semin. Dial.* 23 (5) (2010) 510–515, <https://doi.org/10.1111/j.1525-139X.2010.00770.x>.
- [12] A. Kumar, H.P.J. Schweizer, Bacterial resistance to antibiotics: active efflux and reduced uptake, *Adv. Drug Deliv. Rev.* 57 (10) (2005) 1486–1513, <https://doi.org/10.1016/j.addr.2005.04.004>.
- [13] Prandoni Paolo, Sergio Siragusa, Girolami Bruno, F. Fabrizio, The incidence of heparin-induced thrombocytopenia in medical patients treated with low-molecular-weight heparin: a prospective cohort study, *Blood* 106 (9) (2005) 3049–3054, <https://doi.org/10.1182/blood-2005-03-0912>.
- [14] M.H. Mendler, B. Turlin, R. Moirand, A.M. Jouanolle, T. Sapey, D. Guyader, J.Y. Le Gall, P. Brissot, V. David, Y. Deugnier, A. Insulin resistance-associated hepatic iron overload, *Gastroenterology* 117 (5) (1999) 1155–1163, [https://doi.org/10.1016/S0016-5085\(99\)70401-4](https://doi.org/10.1016/S0016-5085(99)70401-4).
- [15] H.M. Ehmman, D. Breitwieser, S. Winter, C. Gspan, G. Koraimann, U. Maver, M. Segal, K. Köstler, K. Stana-Kleinschek, S. Spirk, Gold nanoparticles in the engineering of antibacterial and anticoagulant surfaces, *Carbohydr. Polym.* 117 (2015) 34–42, <https://doi.org/10.1016/j.carbpol.2014.08.116>.
- [16] J. Wang, M. Qiu, Z. Liu, C. He, Fabrication of a dual-action membrane with both antibacterial and anticoagulant properties via cationic polyelectrolyte-induced phase separation, *ACS Appl. Mater. Interfaces* 13 (13) (2021) 14938–14950, <https://doi.org/10.1021/acsami.1c00256>.
- [17] J. Zhang, X. Ke, M. Huang, X. Pei, S. Gao, D. Wu, J. Chen, Y. Weng, NO released via both a Cu-MOF-based donor and surface-catalyzed generation enhances anticoagulation and antibacterial surface effects, *Biomater. Sci.* 11 (1) (2023) 322–338, <https://doi.org/10.1039/D2BM01515C>.
- [18] Y. Zou, Y. Zhang, Q. Yu, H. Chen, Technology, Dual-function antibacterial surfaces to resist and kill bacteria: painting a picture with two brushes simultaneously, *J. Mater. Sci. Technol.* 70 (2021) 24–38, <https://doi.org/10.1016/j.jmst.2020.07.028>.
- [19] D. Mitra, E.-T. Kang, K.G. Neoh, Polymer-based coatings with integrated antifouling and bactericidal properties for targeted biomedical applications, *ACS Appl. Polym. Mater.* 3 (5) (2021) 2233–2263, <https://doi.org/10.1021/acscpm.1c00125>.
- [20] D. Campoccia, L. Montanaro, C. Arciola, R. Guildford, A review of the biomaterials technologies for infection-resistant surfaces, *Biomaterials* 34 (34) (2013) 8533–8554, <https://doi.org/10.1016/j.biomaterials.2013.07.089>.
- [21] M. Mahmoudi, V. Serpooshan, Silver-coated engineered magnetic nanoparticles are promising for the success in the fight against antibacterial resistance threat, *ACS Nano* 6 (3) (2012) 2656–2664, <https://doi.org/10.1021/nn300042m>.
- [22] W. Dan, H. Markus, G. Yuan, M. Jingzhi, S. Ya, Antibiofilm peptides against biofilms on titanium and hydroxyapatite surfaces, *Bioact. Mater.* 3 (4) (2018) 418–425, <https://doi.org/10.1016/j.bioactmat.2018.06.002>.
- [23] J. Shu, C. Wu, Y. Wu, Z. Li, S. Shao, W. Zhao, X. Tang, H. Yang, L. Shen, X. Zuo, Induction of pluripotency in mouse somatic cells with lineage specifiers, *Cell* 153 (5) (2015) p963–p975, <https://doi.org/10.1016/j.cell.2013.05.001>.
- [24] J. Zhang, D. Wang, X. Jiang, L. He, L. Fu, Y. Zhao, Y. Wang, H. Mo, J. Shen, Multistructured vascular patches constructed via layer-by-layer self-assembly of heparin and chitosan for vascular tissue engineering applications, *Chem. Eng. J.* 370 (2019) 1057–1067, <https://doi.org/10.1016/j.cej.2019.03.270>.
- [25] H. Yu, H. Qiu, W. Ma, M.F. Maitz, Q. Tu, K. Xiong, J. Chen, N. Huang, Z.L. Yang, Endothelium-mimicking surface combats thrombosis and biofouling via synergistic long-and short-distance defense strategy, *Small* 17 (24) (2021), 2100729, <https://doi.org/10.1002/sml.202100729>.
- [26] S. Lee, Janos Voros, An aqueous-based surface modification of poly(dimethylsiloxane) with poly(ethylene glycol) to prevent biofouling, *Langmuir* 21 (25) (2005) 11957–11962, <https://doi.org/10.1021/la051932p>.
- [27] Y.N. Chou, A. Venault, C.H. Cho, M.C. Sin, L.C. Yeh, J.F. Jhong, A. Chinnathambi, Y. Chang, Y. Chang, Colloids, epoxytated zwitterionic triblock copolymers grafted onto metallic surfaces for general biofouling mitigation, *Langmuir* 33 (38) (2017) 9822–9835, <https://doi.org/10.1021/acs.langmuir.7b02164>.
- [28] S. Kim, Y. Jang, L.K. Jang, S.H. Sunwoo, T.I. Kim, S.W. Cho, J.Y. Lee, Electrochemical deposition of dopamine–hyaluronic acid conjugates for anti-biofouling bioelectrodes, *J. Mater. Chem. B* 5 (2017) 4507, <https://doi.org/10.1039/c7tb00028f>.
- [29] Niu Yanlian, Chu Meilin, Xu Ping, Meng Shuangshuang, Zhou Qian, Zhao Bo, Jian Shen, An aptasensor based on heparin-mimicking hyperbranched polyester with anti-biofouling interface for sensitive thrombin detection, *Biosens. Bioelectron.* 101 (2018) 174–180, <https://doi.org/10.1016/j.bios.2017.10.037>.
- [30] P. Lin, C.W. Lin, R. Mansour, F. Gu, Improving biocompatibility by surface modification techniques on implantable bioelectronics, *Biosens. Bioelectron.* 47 (15) (2013) 451–460, <https://doi.org/10.1016/j.bios.2013.01.071>.
- [31] I. Banerjee, R.C. Pangule, R.S. Kane, Antifouling coatings: recent developments in the design of surfaces that prevent fouling by proteins, bacteria, and marine organisms, *Adv. Mater.* 23 (6) (2011), <https://doi.org/10.1002/adma.201001215>.
- [32] D. Zhang, Q. Chen, C. Shi, M. Chen, K. Ma, J. Wan, R. Liu, Dealing with the foreign-body response to implanted biomaterials: strategies and applications of new materials, *Adv. Funct. Mater.* 31 (6) (2020), 2007226, <https://doi.org/10.1002/adfm.202007226>.
- [33] M.A. Daeschel, Y. Zhao, Lysozyme and its antimicrobial application in foods and beverages 237, 2009, p. 67, 67.
- [34] J. Sibarani, M. Takai, K.J.C. Ishihara, Surface modification on microfluidic devices with 2-methacryloyloxyethyl phosphorylcholine polymers for reducing unfavorable protein adsorption, *Colloids Surf. B Biointerfaces* 54 (1) (2007) 88–93, <https://doi.org/10.1016/j.colsurfb.2006.09.024>.
- [35] H. Yu, S. Yu, H. Qiu, P. Gao, Y. Chen, X. Zhao, Q. Tu, M. Zhou, L. Cai, N. Huang, Nitric oxide-generating compound and bio-clickable peptide mimic for synergistically tailoring surface anti-thrombogenic and anti-microbial dual-functions, *Bioact. Mater.* 6 (6) (2021) 1618–1627, <https://doi.org/10.1016/j.bioactmat.2020.11.011>.
- [36] Z. Yang, X. Zhao, R. Hao, Q. Tu, X. Tian, Y. Xiao, K. Xiong, M. Wang, Y. Feng, N. Huang, Bioclickable and mussel adhesive peptide mimics for engineering vascular stent surfaces, *Proc. Natl. Acad. Sci. USA* 117 (28) (2020) 16127–16137, <https://doi.org/10.1073/pnas.2003732117>.
- [37] Y. Yang, P. Gao, J. Wang, Q. Tu, L. Bai, K. Xiong, H. Qiu, X. Zhao, M.F. Maitz, H. Wang, Endothelium-mimicking multifunctional coating modified cardiovascular stents via a stepwise metal-catechol-(amine) surface engineering strategy, *Research* 2020 (2020), 9203906, <https://doi.org/10.34133/2020/9203906>.
- [38] H. Olzscha, S.M. Schermann, A.C. Woerner, S. Pinkert, M.H. Hecht, G.G. Tartaglia, M. Vendruscolo, M. Hayer-Hartl, F.U. Hartl, Amyloid-like aggregates sequester numerous metastable proteins with essential cellular functions, *Cell* 144 (1) (2011) p67–p78, <https://doi.org/10.1016/j.cell.2010.11.050>.
- [39] D. Wang, Y. Ha, J. Gu, Q. Li, L. Zhang, P. Yang, 2D protein supramolecular nanofilm with exceptionally large area and emergent functions, *Adv. Mater.* 28 (34) (2016) 7414–7423, <https://doi.org/10.1002/adma.201506476>.
- [40] J. Tian, Y. Liu, S. Miao, Q. Yang, X. Hu, Q. Han, L. Xue, P.J.B.S. Yang, Amyloid-like protein aggregates combining antifouling with antibacterial activity, *Biomater. Sci.* 8 (24) (2020) 6903–6911, <https://doi.org/10.1016/j.cel.2010.11.050>.
- [41] L. Li, G. Li, Y. Wu, Y. Lin, Y. Qu, Y. Wu, K. Lu, Y. Zou, H. Chen, Q. Yu, Technology, Dual-functional bacterial cellulose modified with phase-transitioned proteins and gold nanorods combining antifouling and photothermal bactericidal properties, *J. Mater. Sci. Technol.* 110 (2022) 14–23, <https://doi.org/10.1016/j.jmst.2021.10.011>.
- [42] Y. Qu, X. Zhu, R. Kong, K. Lu, T. Fan, Q. Yu, G. Wang, Dual-functional antibacterial hybrid film with antifouling and NIR-activated bactericidal properties, *Compos. B Eng.* 244 (2022), 110143, <https://doi.org/10.1016/j.compositesb.2022.110143>.

- [43] G. Sancataldo, V. Vetri, V. Foderà, G.D. Cara, V. Militello, M. Leone, Oxidation enhances human serum albumin thermal stability and changes the routes of amyloid fibril formation, *PLoS One* 9 (1) (2014), e84552, <https://doi.org/10.1371/journal.pone.0084552>.
- [44] B. Saif, W. Zhang, X. Zhang, Q. Gu, P. Yang, Sn-triggered two-dimensional fast protein assembly with emergent functions, *ACS Nano* 13 (7) (2019), <https://doi.org/10.1021/acsnano.9b01392>.
- [45] T.A. Egorov, Identification of cysteine residues and disulfide bonds in proteins, *Protein Structure Analysis* (1997) 259–268. [https://link.springer.com/chapter/10.1007/978-3-642-59219-5\\_17](https://link.springer.com/chapter/10.1007/978-3-642-59219-5_17).
- [46] Y. Xu, Y. Liu, X. Hu, R. Qin, H. Su, J. Li, P. Yang, The synthesis of a 2D ultra-large protein supramolecular nanofilm by chemoselective thiol–disulfide exchange and its emergent functions, *Angew. Chem. Int. Ed.* 59 (7) (2020) 2850–2859, <https://doi.org/10.1002/anie.201912848>.
- [47] D. Essassi, R. Zini, J.P. Tillement, Use of 1-anilino-8-naphthalene sulfonate as a fluorescent probe in the investigation of drug interactions with human alpha-1-acid glycoprotein and serum albumin, *J. Pharmaceut. Sci.* 79 (1) (1990) 9–13, <https://doi.org/10.1002/jps.2600790104>.
- [48] Gao Aiting, Wu Qian, Wang Dehui, Ha Yuan, C.J. Zhijun, A superhydrophobic surface templated by protein self-assembly and emerging application toward protein crystallization, *Adv. Mater.* 28 (3) (2016) 579–587, <https://doi.org/10.1002/adma.201504769>.
- [49] C. Liu, J. Lee, J. Ma, Elimelech, M.J.E. Science, Technology, antifouling thin-film composite membranes by controlled architecture of zwitterionic polymer brush layer, *Environ. Sci. Technol.* (2017), <https://doi.org/10.1021/acs.est.6b05992>.
- [50] J. Wang, W. Gao, H. Zhang, M. Zou, Y. Chen, Y. Zhao, Programmable wettability on photocontrolled graphene film, *Sci. Adv.* 4 (9) (2018), eaat7392, <https://doi.org/10.1126/sciadv.aat7392>.
- [51] Li Chen, Yu mei Wen, The role of bacterial biofilm in persistent infections and control strategies, *Int. J. Oral Sci.* (3) (2011) 66–73, <https://doi.org/10.4248/IJOS11022>.
- [52] B. Song, E. Zhang, X. Han, H. Zhu, Y. Shi, Z. Cao, Interfaces, engineering and application perspectives on designing an antimicrobial surface, *ACS Appl. Mater. Interfaces* 12 (19) (2020) 21330–21341, <https://doi.org/10.1021/acsami.9b19992>.
- [53] H.L.D. Leij, How does lysozyme penetrate through the bacterial outer membrane? *Biochim. Biophys. Acta Nucleic Acids Protein Synth.* 443 (3) (1976) 534–544, [https://doi.org/10.1016/0005-2787\(76\)90515-3](https://doi.org/10.1016/0005-2787(76)90515-3).
- [54] W. Li, X. Yang, P. Lai, L. Shang, Bio-inspired adhesive hydrogel for biomedicine—principles and design strategies, *Smart Med.* 1 (1) (2022), e20220024, <https://doi.org/10.1002/SMMD.20220024>.
- [55] S. Mieszkina, P. Martin-Tanchereau, M.E. Callow, J.A. Callow, Effect of bacterial biofilms formed on fouling-release coatings from natural seawater and *Cobetia marina*, on the adhesion of two marine algae, *Biofouling* 28 (9) (2012) 953–968, <https://doi.org/10.1080/08927014.2012.723696>.
- [56] X. Mou, H. Zhang, H. Qiu, W. Zhang, Y. Wang, K. Xiong, N. Huang, H.A. Santos, Z. Yang, Mussel-inspired and bioclickable peptide engineered surface to combat thrombosis and infection, *Research* 2022 (2022), 9780879, <https://doi.org/10.34133/2022/9780879>.